The transcriptional corepressor CTBP-1 acts with the SOX family transcription factor EGL-13 to maintain AIA interneuron cell identity in *C. elegans*

Josh Saul[1], Takashi Hirose[1,#a], H. Robert Horvitz[1,*]

Affiliations

[1] Howard Hughes Medical Institute, Department of Biology, Massachusetts Institute of Technology, Cambridge, MA, USA

[#a] Current Address: Sysmex Corporation, 4-4-4 Takatsukadai, Nishi-ku, Kobe 651-2271, Japan

*Corresponding author

email: horvitz@mit.edu (HRH)

Draft: 10/6/2021

Abstract

Cell identity is characterized by a distinct combination of gene expression, cell morphology and cellular function established as progenitor cells divide and differentiate. Following establishment, cell identities can be unstable and require active and continuous maintenance throughout the remaining life of a cell. Mechanisms underlying the maintenance of cell identities are incompletely understood. Here we show that the gene *ctbp-1,* which encodes the transcriptional corepressor C-terminal binding protein-1 (CTBP-1), is essential for the maintenance of the identities of the two AIA interneurons in the nematode *Caenorhabditis elegans*. *ctbp-1* is not required for the establishment of the AIA cell fate but rather functions cell-autonomously and can act in later larval stage and adult worms to maintain proper AIA gene expression, morphology and function. From a screen for suppressors of the *ctbp-1* mutant phenotype, we identified the gene *egl-13,* which encodes a SOX family transcription factor. We found that *egl-13* regulates AIA function and aspects of AIA gene expression, but not AIA morphology. We conclude that the CTBP-1 protein maintains AIA cell identity in part by utilizing EGL-13 to repress transcriptional activity in the AIAs. More generally, we propose that transcriptional corepressors like CTBP-1 might be critical factors in the maintenance of cell identities, harnessing the DNA-binding specificity of transcription factors like EGL-13 to selectively regulate gene expression in a cell-specific manner.

Introduction

Over the course of animal development, complex networks of transcription factors act and interact to drive the division and differentiation of progenitor cells towards terminal cell identities [1–8]. These networks of transcriptional activity often culminate in the activation of master transcriptional regulators that are responsible for directing the differentiation of a diverse range of cell and tissue types [4,9–12]. Examples of such master transcriptional regulators include the mammalian bHLH transcription factor MyoD, which specifies skeletal muscle cells [13–15]; the *Drosophila* Pax-family transcription factor Eyeless, which drives differentiation of the fly eye [16–20]; and the *C. elegans* GATA transcription factor ELT-2, essential for development of the worm intestine [21–24]. Many such master transcriptional regulators are not only required to establish the identities of specific cell types but are subsequently continuously required to maintain those identities for the remaining life of the cell [4,23,25–29]. Defects in the maintenance of cell identities can manifest as late-onset misregulated gene expression, altered morphology or disrupted cellular function, and often become progressively worse as the cell ages [25,28,30–32].

Previous studies of the nematode *Caenorhabditis elegans* have identified a class of master transcriptional regulators, termed terminal selectors [4,12,33–37]. Terminal selectors drive the expression of whole batteries of gene activity that ultimately define the unique features of many different cell types [10–12]. Individual terminal selectors have been shown to contribute to the establishment and maintenance of multiple distinct *C. elegans* cell types and to drive the

62 expression of many cell-type specific genes [7,37–41]. However, it has been
63 unclear how individual terminal selectors can drive the expression of cell-type
64 specific genes in only the appropriate cell types rather than in all cells in which
65 they act [42–44]. Recent work has shown that terminal selectors appear to
66 broadly activate the expression of many genes, including cell-type specific
67 genes, in all cells in which they function [42,45]. Piecemeal assemblies of
68 transcription factors are then responsible for pruning this broad expression to
69 restrict expression of cell-type specific genes to the appropriate cell types
70 [42,45]. This restriction of the activation of gene expression by terminal selectors
71 appears to be an essential aspect of proper cell-identity maintenance
72 [28,42,45,46]. However, it is not known how the myriad of transcription factors
73 utilized to restrict terminal selector gene activation are coordinated and
74 controlled.

75 Here we report the discovery that the *C. elegans* gene *ctbp-1,* which
76 encodes the sole worm ortholog of the C-terminal Binding Protein (CtBP) family
77 of transcriptional corepressors [47–55], functions to maintain the cell identity of
78 the two AIA interneurons. We demonstrate that CTBP-1 functions with the SOX-
79 family transcription factor EGL-13 [56,57] to maintain multiple aspects of the AIA
80 cell identity and propose that CTBP-1 does so in part by utilizing EGL-13 to
81 repress transcriptional activity in the AIAs.

82 ## Results

83 **Mutations in *ctbp-1* cause *ceh-28* reporter misexpression in the AIA**
84 **neurons**

85 In previous studies, we screened for and characterized mutations that
86 prevent the programmed cell death of the sister cell of the *C. elegans* M4 neuron
87 [58,59]. For these screens, we used the normally M4-specific GFP transcriptional
88 reporter $P_{ceh\text{-}28}$*::gfp* and identified isolates with an undead M4 sister cell, which
89 expresses characteristics normally expressed by the M4 cell, on the basis of
90 ectopic GFP expression. In addition to mutants with an undead M4 sister cell, we
91 isolated 18 mutant strains that express $P_{ceh\text{-}28}$*::gfp* in a manner uncharacteristic
92 of M4 or its undead sister. These mutants express $P_{ceh\text{-}28}$*::gfp* in a bilaterally
93 symmetric pair of cells located near the posterior of the *C. elegans* head, far from
94 both M4 and the single M4 sister cell (Fig. 1A).

95 These mutations define a single complementation group and all 18 mutant
96 strains have mutations in the transcriptional corepressor gene *ctbp-1* (Figs. 1C;
97 S1A-B; S2A). These *ctbp-1* alleles include three splice-site mutations and nine
98 nonsense mutations (such as the mutation *n4784,* an early nonsense mutation
99 and one of many presumptive null alleles of the gene). The mutant phenotype is
100 recessive, and a transgenic construct carrying a wild-type copy of *ctbp-1*
101 expressed under its native promoter fully rescued the GFP misexpression
102 caused by *n4784* (Figs. 1A; S2A). *tm5512*, a 632 bp deletion spanning the
103 transcription start site and first two exons of the *ctbp-1a* isoform and a
104 presumptive null allele of this gene [60], likewise caused $P_{ceh\text{-}28}$*::gfp*

105 misexpression in two cells in the posterior region of the head (Fig. S1C-D),
106 similar to our *ctbp-1* isolates. These findings demonstrate that loss of *ctbp-1*
107 function is responsible for $P_{ceh\text{-}28}$*::gfp* misexpression.

108 To determine the identity of the cells misexpressing the normally M4-
109 specific marker $P_{ceh\text{-}28}$*::gfp*, we examined reporters for cells in the vicinity of the
110 observed misexpression in *ctbp-1* mutants. The AIA-neuron reporter *nIs843[*$P_{gcy\text{-}}$
111 $_{28.d}$*::mCherry]* showed complete overlap with misexpressed $P_{ceh\text{-}28}$*::gfp*, indicating
112 that the cells misexpressing the M4 reporter are the two bilaterally symmetric and
113 embryonically-generated AIA interneurons (Fig. 1B).

114

115 **The penetrance of *ceh-28* reporter misexpression in the AIA neurons**
116 **increases with age**

117 While characterizing *ctbp-1* mutants, we noticed that fewer young worms
118 misexpress $P_{ceh\text{-}28}$*::gfp* in the AIAs than do older worms (Fig. 1D). To investigate
119 the temporal aspect of this phenotype, we scored *ctbp-1* mutants for $P_{ceh\text{-}28}$*::gfp*
120 misexpression throughout the four worm larval stages (L1-L4) and into the first
121 day of adulthood ("early" and "day 1" adults). *ctbp-1* mutants rarely misexpressed
122 $P_{ceh\text{-}28}$*::gfp* at early larval stages, but displayed an increasing penetrance, though
123 invariant expressivity, of this defect as worms transitioned through larval
124 development, such that by the last larval stage (L4) nearly all worms exhibited
125 reporter misexpression specifically and solely in the AIAs (Fig. 1E). A similar
126 stage-dependent increase in reporter expression in *ctbp-1* mutants occurred in
127 mutants carrying a second independently-generated *ceh-28* reporter, *nIs348[*$P_{ceh\text{-}}$

128 $_{28}$*::mCherry]* (Fig. S1E). These results demonstrate that *ctbp-1* function prevents
129 an age-dependent misexpression of the M4-specific gene *ceh-28* in the unrelated
130 AIA neurons.

131 We next asked in what cells and at what stages *ctbp-1* functions to
132 suppress $P_{ceh\text{-}28}$*::gfp* expression in the AIAs. We generated a transgenic
133 construct that expresses wild-type *ctbp-1* specifically in the AIAs, *nIs743[*$P_{gcy\text{-}}$
134 $_{28.d}$*::ctbp-1(+)]* (hereafter referred to as *nIs743[*P_{AIA}*::ctbp-1(+)]*). We found that
135 AIA-specific restoration of *ctbp-1* was sufficient to suppress $P_{ceh\text{-}28}$*::gfp*
136 misexpression in an otherwise *ctbp-1* mutant background (Figs. 1F; S2A),
137 demonstrating that *ctbp-1* is able to act cell-autonomously to regulate *ceh-28*
138 expression in the AIA neurons.

139 To determine if *ctbp-1* can act in older animals to suppress AIA gene
140 misexpression, we generated a transgenic construct that drives expression of
141 wild-type *ctbp-1* throughout the worm in response to a short heat shock,
142 *nEx2351[*$P_{hsp\text{-}16.2}$*::ctbp-1(+);*$P_{hsp\text{-}16.41}$*::ctbp-1(+)]* (hereafter referred to as
143 *nEx2351[*P_{hsp}*::ctbp-1(+)]*). We found that heat shock during the L4 larval stage
144 was sufficient to suppress $P_{ceh\text{-}28}$*::gfp* misexpression in adult *ctbp-1* mutant AIAs
145 (Figs. 1G-H; S2B), demonstrating that *ctbp-1* can act in L4-to-young adult stage
146 worms to regulate AIA gene expression.

147 From these data we conclude that *ctbp-1* is able to act cell-autonomously
148 and in L4-to-young adult worms to prevent expression of at least one non-AIA
149 gene in the AIA neurons.

150

151 ***ctbp-1* mutant AIAs are not transdifferentiating into an M4-like cell identity**

152 We asked if $P_{ceh\text{-}28}$*::gfp* misexpression in the AIAs of *ctbp-1* mutants might
153 be a consequence of the AIAs transdifferentiating into an M4-like cell identity. We
154 scored *ctbp-1* mutants for cell-type markers expressed in, although not
155 necessarily unique to, either M4 or the AIA neurons (Figs. 2A-B; S3A-B). We
156 found that *ctbp-1* mutant AIAs expressed all five of five AIA markers tested and
157 did not express any of four other (non-*ceh-28)* M4 markers tested. Of particular
158 note, *ctbp-1* mutant AIAs did not misexpress either of the two tested M4 genes
159 known to be directly regulated by *ceh-28* (i.e. *dbl-1* and *egl-17)*, indicating that
160 the *ceh-28* misexpression in mutant AIAs does not activate the *ceh-28* regulatory
161 pathway [61,62]. We conclude that *ctbp-1* mutant AIAs are not transdifferentiated
162 into M4-like cells and instead seem to retain much of their AIA identity while
163 gaining at least one M4 characteristic (i.e. *ceh-28* expression) later in life.
164

165 ***ctbp-1* mutants display an increasingly severe disruption of AIA**
166 **morphology**

167 Because of the time-dependency of the defect of *ctbp-1* mutants in AIA
168 cell identity, we hypothesized that *ctbp-1* might act to maintain the AIA cell
169 identity. To test this hypothesis, we examined morphological and functional
170 aspects of AIA identity at both early and late larval stages. To assay AIA
171 morphology, we generated a transgenic construct driving expression of GFP
172 throughout the AIA cell (*nIs840[*$P_{gcy\text{-}28.d}$*::gfp]*). We crossed this construct into
173 *ctbp-1* mutant worms and visualized AIA morphology in L1 and L4 larvae as well

174 as in day 1 adults (Fig. 3A). We found that L1 *ctbp-1* mutant AIAs appeared
175 grossly wild-type in morphology (Fig. 3A). However, L4 and adult *ctbp-1* mutant
176 AIAs had ectopic neurite branches that extended from both the anterior and
177 posterior ends of the AIA cell body (Fig. 3A). The penetrance of these ectopic
178 branches increased progressively in later larval stage and adult mutants (Fig. 3B-
179 C). Older *ctbp-1* mutant AIAs also appeared to have an elongated cell body
180 compared to wild-type AIAs. Quantification of this defect revealed that L4 and
181 adult mutant AIA cell bodies, but not those of L1s, were significantly longer than
182 their wild-type counterparts (Fig. 3D). To assess if this increase in AIA length was
183 a consequence of an increase in AIA size, we measured the maximum area of
184 the AIA cell body from cross-sections of these cells. We found that the maximum
185 area of the AIA cell body did not significantly differ between wild-type and mutant
186 AIAs at any stage (Fig. S4A), indicating that mutant AIAs were misshapen but not
187 enlarged. To confirm that we were not biased by an awareness of genotype while
188 measuring AIA lengths, we blinded the wild-type and *ctbp-1* AIA images used for
189 length measurements and scored the blinded images as either “normal” or
190 “elongated” (Fig. S4B). Again, at the L1 larval stage both wild-type and *ctbp-1*
191 mutant AIAs appeared overwhelmingly “normal,” whereas at both the L4 larval
192 stage and in day 1 adults *ctbp-1* mutant AIAs were scored as “elongated” at a
193 consistently higher rate than their wild-type counterparts. Collectively, these
194 results demonstrate that *ctbp-1* mutant AIAs display abnormal morphology and
195 that the severity of the observed morphological defects in *ctbp-1* mutants
196 increases from L1 to L4 to adulthood. Furthermore, the relative lack of AIA

197 morphological defects in L1 *ctbp-1* mutants suggests that *ctbp-1* is not required
198 for the establishment of proper AIA morphology but instead acts to maintain AIA
199 morphology over time.

200 We next asked if *ctbp-1* acts cell-autonomously and at later stages to
201 regulate AIA morphology as it does for AIA gene expression. We visualized *ctbp-*
202 *1* mutant AIAs carrying the AIA-specific *ctbp-1(+)* rescue construct
203 *nIs743[P_{AIA}::ctbp-1(+)]* (Fig. 3E). We found that AIA-specific restoration of *ctbp-1*
204 in mutant worms rescued all AIA morphological defects to near-wild-type levels at
205 all stages tested, indicating that *ctbp-1* can act cell-autonomously to regulate AIA
206 morphology (Fig. 3F-H). Next, we visualized *ctbp-1* mutant worms carrying the
207 heat shock-inducible *ctbp-1(+)* rescue construct *nEx2351[P_{hsp}::ctbp-1(+)]*. We
208 found that heat shock at the L4 stage did not restore *ctbp-1* mutant AIA
209 morphology in day 1 adults back to wild-type, nor was there any significant
210 difference in the frequency of morphological defects between heat-shocked and
211 non-heat-shocked adults carrying the rescue construct (Fig. 3I-L). We speculate
212 that the lack of restoration of morphology in late-stage worms might be a
213 consequence of the defects being irreversible, and that *ctbp-1* might be
214 continuously required to prevent such defects from occurring. From these data
215 we conclude that *ctbp-1* can act cell-autonomously, and possibly continuously, to
216 maintain aspects of AIA morphology in a manner similar to AIA gene expression.
217

218 **_ctbp-1_ mutants display a progressive decline of AIA function**

219 The AIA interneurons integrate sensory information from a number of
220 sensory neurons, resulting in modulation of the movement of the worm in
221 response to environmental stimuli [63–65]. The AIAs function in response to
222 volatile odors and play an important role in learning associated with the sensation
223 of volatile odors or salts [63,66]. We asked if *ctbp-1* mutants are abnormal in a
224 behavior known to require the AIAs – adaptation to the volatile odor 2-butanone
225 [66] – reasoning that if AIA function is disrupted in *ctbp-1* mutants, there should
226 be a reduction of adaptation (and thus greater attraction) to butanone in *ctbp-1*
227 worms relative to wild-type worms.
228 Consistent with previous studies [66], we found that worms that had been
229 briefly starved with 90 minutes of food deprivation and had no prior experience
230 with butanone (so-called "naïve" worms) were generally attracted to the odor,
231 while worms that were briefly starved in the presence of butanone ("conditioned"
232 worms) adapted to the odor and exhibited mild repulsion to it (Fig. 4A-E). We
233 next compared wild-type and *ctbp-1* mutant worms for their ability to adapt to
234 butanone. We found that while L1 *ctbp-1* worms showed an ability to adapt to
235 butanone roughly similar to that of their wild-type counterparts, conditioned L4
236 *ctbp-1* mutants displayed a significant decrease in repulsion from butanone
237 relative to wild-type L4 animals, indicating a decrease in their ability to adapt to
238 the odor (Fig. 4B-E). As a control, we assayed a strain carrying a transgenic
239 construct that genetically ablates the AIA neurons, JN580. As expected, JN580
240 worms displayed decreased butanone adaptation at both the L1 and L4 larval
241 stages. Thus, *ctbp-1* mutant worms displayed a defect in butanone adaptation

242 similar to that of an AIA-ablated strain and did so only at a later larval stage,
243 suggesting a potential loss of AIA function in L4 *ctbp-1* mutants. However, while
244 *ctbp-1* mutant L4s exhibited weaker butanone adaptation than their wild-type
245 counterparts, this defect was not as severe as that of JN580 L4s, indicating that
246 *ctbp-1* mutant AIAs might retain some function. Additionally, the lack of a
247 butanone adaptation defect in L1 *ctbp-1* mutants similar to that of L1 JN580
248 worms further suggests that loss of *ctbp-1* does not disrupt early AIA function
249 and shows that *ctbp-1* is not required for the establishment of functional AIA
250 neurons.

251 We next asked if *ctbp-1* can act cell-autonomously in the AIAs and in older
252 worms to regulate butanone adaptation. We assayed *ctbp-1* mutants carrying the
253 AIA-specific rescue construct *nIs743[*P_{AIA}*::ctbp-1(+)]* for butanone adaptation
254 (Fig. 4B-E) and found that AIA-specific restoration of *ctbp-1* rescued butanone
255 adaption of conditioned *ctbp-1* mutant L4s to near wild-type levels (Fig. 4E). We
256 conclude that the butanone adaptation defect of *ctbp-1* mutants is caused by a
257 disruption of AIA function and that *ctbp-1* can act cell-autonomously to regulate
258 this AIA function. Next, we assayed *ctbp-1* mutants carrying the heat shock-
259 inducible *ctbp-1(+)* rescue construct *nEx2351[*P_{hsp}*::ctbp-1(+)]* for butanone
260 adaptation. We found that restoration of *ctbp-1* by heat shock at the L4 larval
261 stage rescued the butanone adaptation defect in day 1 adults, indicating that
262 *ctbp-1* can act in L4-to-day 1 adult worms to maintain proper AIA function after
263 the initial establishment of the AIA cell identity (Fig. 4F-G). Taken together, these
264 data establish that loss of *ctbp-1* disrupts the function of the AIA neurons and

265 that *ctbp-1* can act cell-autonomously and in L4-to-day 1 adult worms to maintain
266 AIA function.
267 While conducting these assays, we observed that naïve *ctbp-1* mutant
268 worms displayed a mildly weaker attraction to butanone than did their wild-type
269 counterparts at both the L1 and L4 larval stages (Fig. 4B,D). AIA-specific rescue
270 of *ctbp-1* did not rescue this mild chemotaxis defect – naïve *ctbp-1* mutants
271 carrying the P_{AIA}*::ctbp-1(+)* construct still displayed weaker butanone attraction
272 than wild-type worms (Fig. 4B,D). We suggest that this defect in attraction to
273 butanone is not a consequence of dysfunction of the AIAs but rather of some
274 other cell(s) involved in butanone chemotaxis. Consistent with this hypothesis,
275 we found that *ctbp-1* mutants were defective in chemotaxis to the volatile odor
276 isoamyl alcohol but were not defective in the response to diacetyl (Fig. S5A-B)
277 while AIA-ablated strain JN580 animals were not defective in either response
278 (Fig. S5A-B). These observations indicate that *ctbp-1* mutant worms have a
279 broader defect in chemotaxis caused by the disruption of the function of cells
280 other than the AIAs. Because our primary focus has been on how *ctbp-1*
281 functions to maintaining the AIA cell identity, we did not attempt to identify the
282 other cells with functions perturbed by the loss of *ctbp-1*.
283
284 ***ctbp-1* mutant AIAs have additional defects in gene expression**
285 To better characterize the genetic changes occurring in mutant AIAs, we
286 performed a single, exploratory single-cell RNA-Sequencing (scRNA-Seq)
287 experiment comparing wild-type and *ctbp-1* mutant worms. We sequenced RNA

288 from the neurons of wild-type and *ctbp-1* L4 worms and processed the resulting
289 data using the 10X CellRanger pipeline to identify presumptive AIA neurons
290 based on the expression of several AIA markers (*gcy-28*, *ins-1*, *cho-1*) shown
291 above to be expressed in both wild-type and *ctbp-1* mutant AIAs (Fig. 2B).
292 Confirming that these data captured changes in the AIA transcriptional profiles,
293 we found that *ctbp-1* mutant AIAs showed high levels of expression of *ceh-28,*
294 while wild-type AIAs showed no detectable *ceh-28* expression (Fig. S6).
295 We analyzed AIA transcriptional profiles to identify genes that appeared to
296 be either expressed in *ctbp-1* mutant AIAs and not expressed in wild-type AIAs
297 (similar to *ceh-28*) or expressed in wild-type AIAs but not expressed in *ctbp-1*
298 AIAs. To confirm candidate genes, we crossed existing reporters for those genes
299 to *ctbp-1* mutants or, in cases for which reporters were not readily available,
300 generated our own transgenic constructs. We identified and confirmed one gene
301 that, similar to *ceh-28*, was not expressed in wild-type AIAs but was
302 misexpressed in *ctbp-1* mutant AIAs: *acbp-6*, which is predicted to encode an
303 acyl-Coenzyme A binding protein [67] (Fig. 5A; S6). We also identified and
304 confirmed two genes expressed in wild-type AIAs but not expressed in *ctbp-1*
305 mutant AIAs: *sra-11*, which encodes a transmembrane serpentine receptor [68];
306 and *glr-2,* which encodes a glutamate receptor [69] (Fig. 5C,E; S6). We
307 visualized the *acbp-6* reporter *nEx3081[*$P_{acbp\text{-}6}$*::gfp]*, the *sra-11* reporter
308 *otIs123[*$P_{sra\text{-}11}$*::gfp]* and the *glr-2* reporter *ivEx138[*$P_{glr\text{-}2}$*::gfp]* in wild-type and
309 *ctbp-1* L4 worms and confirmed that *acbp-6* was absent in wild-type AIAs but
310 misexpressed in *ctbp-1* mutants (Fig. 5A-B), while both *sra-11* and *glr-2* were

311 consistently expressed in wild-type AIAs but not expressed in the AIAs of *ctbp-1*
312 mutants (Fig. 5C-F). We also visualized these reporters in L1 wild-type and *ctbp-*
313 *1* worms and found that both $P_{acbp\text{-}6}$*::gfp* and $P_{sra\text{-}11}$*::gfp* displayed a time-
314 dependence to their expression similar to that of $P_{ceh\text{-}28}$*::gfp* − $P_{acbp\text{-}6}$*::gfp* was
315 rarely detectible in the AIAs of either wild-type of *ctbp-1* AIAs at the L1 stage but
316 was consistently expressed in *ctbp-1* mutant L4 AIAs (Fig. 5A-B), while $P_{sra\text{-}}$
317 $_{11}$*::gfp* was rarely detectible in the AIAs of either wild-type or *ctbp-1* mutant L1
318 worms but was expressed in the AIAs of most wild-type worms by the L4 stage
319 while remaining off in the AIAs of most L4 *ctbp-1* mutants (Fig. 5C-D). These
320 observations suggest that, like *ceh-28* expression, *acbp-6* and *sra-11* expression
321 is regulated by *ctbp-1* primarily in the AIAs of late-stage larvae and adults. By
322 contrast, *glr-2* was expressed in wild-type but not *ctbp-1* AIAs in both L1 and L4
323 larvae (Fig. 5E-F).
324 These data demonstrate that mutant AIAs fail to turn on and/or maintain
325 the expression of genes characteristic of the adult AIA neuron (*sra-11* and *glr-2*)
326 while misexpressing at least two genes uncharacteristic of AIA (*ceh-28* and *acbp-*
327 *6)*. That the majority of these abnormalities in AIA gene expression occurred long
328 after the AIAs are generated during embryogenesis further supports the
329 conclusion that *ctbp-1* does not act to establish the AIA cell identity.
330 Collectively, our findings concerning AIA gene expression, morphology
331 and function demonstrate that *ctbp-1* acts to maintain the AIA cell identity, plays
332 little to no role in the initial establishment of the AIA cell fate, and can act cell-
333 autonomously and in older worms to maintain these aspects of the AIA identity.

334

335 ***egl-13* mutations suppress the *ctbp-1* mutant phenotype**

336 To investigate how *ctbp-1* acts to maintain AIA cell identity, we performed
337 a mutagenesis screen for suppression of $P_{ceh\text{-}28}$*::gfp* misexpression in the AIAs of
338 L4 *ctbp-1* mutants (Fig. 6A). Using a combination of Hawaiian SNP mapping [70]
339 and whole-genome sequencing, we identified the gene *egl-13*, which encodes a
340 SOX family transcription factor, as a suppressor of *ctbp-1*. *egl-13* has been
341 shown to act in the establishment of the BAG and URX cell fates and in vulval
342 development of *C. elegans* [56,71], and its mammalian orthologs SOX5 and
343 SOX6 act in neural fate determination [72,73]. We isolated three alleles of *egl-13*
344 as *ctbp-1* suppressors: *n5937*, a mutation of the splice acceptor site at the
345 beginning of the 6th exon of the *egl-13a* isoform resulting in a frameshift and early
346 stop; *n6013*, a Q381ochre nonsense mutation towards the end of the *egl-13*
347 transcript; and *n6313*, a 436-nucleotide deletion spanning the 7th and 8th exons of
348 the *egl-13a* isoform (Figs. 6B; S7A-B). We generated and introduced a
349 transgenic construct carrying a wild-type copy of *egl-13* under its native promoter
350 into these mutant strains and found that this construct was capable of rescuing
351 the suppression of $P_{ceh\text{-}28}$*::gfp* misexpression by all three *egl-13* alleles,
352 demonstrating that loss of *egl-13* function suppresses this aspect of the *ctbp-1*
353 mutant phenotype and suggesting that these alleles are likely loss-of-function
354 alleles of *egl-13* (Fig. S7C).

355 We assayed the loss-of-function allele of *egl-13* with the highest
356 penetrance of suppression*, n5937,* for its ability to suppress $P_{ceh\text{-}28}$*::gfp*

357 misexpression over the course of larval development and into adulthood of *ctbp-*
358 *1* mutant worms (Fig. 6C). *egl-13(n5937)* strongly suppressed *ctbp-1* at all
359 stages, resulting in little to no misexpression of P_{ceh-28}*::gfp* in the AIAs of *egl-13*
360 *ctbp-1* double mutants at any larval stage or in day 1 adults.

361 To determine if, like *ctbp-1*, *egl-13* can act cell-autonomously in the AIAs,
362 we generated a transgenic construct that drives expression of a wild-type copy of
363 *egl-13* in the AIAs (*nEx3055[*$P_{gcy-28.d}$*::egl-13(+)]*). Introduction of this construct to
364 *egl-13(n5937) ctbp-1* double mutants rescued the *egl-13* suppression of P_{ceh-}
365 $_{28}$*::gfp* misexpression in the AIAs, indicating that *egl-13* can function cell-
366 autonomously (Fig. S8A-B). These results suggest that, in the absence of *ctbp-1*
367 function, ectopic *egl-13* activity drives *ceh-28* misexpression, and thus that *ctbp-1*
368 likely normally acts to repress *egl-13* activity in the AIAs.

369 We next asked if *egl-13(n5937)* could suppress the AIA morphological and
370 functional defects of *ctbp-1* mutants. To both test suppression of AIA
371 morphological defects and confirm the presence of the AIA neurons in *egl-13*
372 *ctbp-1* double mutants, we crossed the AIA morphology reporter *nIs840[*P_{gcy-}
373 $_{28.d}$*::gfp]* into *egl-13 ctbp-1* double mutants and scored AIA morphology in L1, L4
374 and day 1 adult worms (Fig. 6D-G). *egl-13 ctbp-1* double mutant AIAs displayed
375 a mild (though significant) reduction in the penetrance of ectopic anterior neurites
376 only in adult worms, no significant change in the frequency of posterior neurites
377 at any stage, and a slight increase in AIA cell body length of L4 worms (though
378 the difference was no longer significant in adults). These data demonstrate that
379 loss of *egl-13* has little consistent effect on the AIA morphological defects caused

380 by a loss of *ctbp-1* activity, suggesting that *ctbp-1* maintains AIA morphology
381 primarily through *egl-13*-independent pathways.
382 We next assayed the ability of *egl-13(n5937)* to suppress AIA functional
383 defects. We tested *egl-13 ctbp-1* double mutants for butanone adaptation and
384 found that, at the L1 larval stage, this double mutant strain displayed a detectable
385 response to butanone similar to *ctbp-1* single mutants (Fig. 6H-I). By contrast, at
386 the L4 larval stage, mutation of *egl-13* strongly suppressed the *ctbp-1* mutant
387 defect in butanone adaptation, causing near wild-type levels of repulsion in
388 conditioned worms (Fig. 6J-K). These results indicate that loss of *egl-13* activity
389 suppressed AIA functional defects of *ctbp-1* mutant worms and suggest that
390 *ctbp-1* maintains at least this aspect of AIA cellular function primarily through an
391 *egl-13*-dependent pathway.
392 From these data we conclude that *ctbp-1* maintains AIA function and at
393 least some aspects of AIA gene expression by antagonizing *egl-13* function and
394 that *ctbp-1* likely also acts primarily through one or more *egl-13*-independent
395 pathways to maintain AIA cellular morphology.
396
397 **_egl-13_ regulates AIA function through control of _ceh-28_ expression**
398 We next asked if mutation of *egl-13* could suppress other *ctbp-1* mutant
399 AIA gene expression defects besides that of *ceh-28*. We crossed in *acbp-6*, *sra-*
400 *11* and *glr-2* reporters to *egl-13 ctbp-1* double mutants and visualized reporter
401 expression at the L1 and L4 larval stages. We found that mutation of *egl-13*
402 suppressed $P_{acbp\text{-}6}$*::gfp* misexpression in the AIAs (Fig. 7A,D, compare to Fig. 5),

403 just as *egl-13* mutation suppressed $P_{ceh\text{-}28}$*::gfp* misexpression. By contrast,
404 mutation of *egl-13* had no effect on the loss of $P_{sra\text{-}11}$*::gfp* or $P_{glr\text{-}2}$*::gfp* expression
405 in *ctbp-1* mutants (Fig. 7B-D). We speculated that EGL-13 might directly regulate
406 expression of *ceh-28* or *acbp-6*. To test this hypothesis, we examined the *ceh-28*
407 and *acbp-6* promoter regions for possible EGL-13 binding sites. We failed to
408 identify any promising candidates, suggesting that regulation of these genes by
409 EGL-13 is likely indirect. These results demonstrate that some, though not all, of
410 the AIA gene expression defects seen in *ctbp-1* mutants are regulated through
411 *egl-13*.
412 As *egl-13* is required for misexpression of both *ceh-28* and *acbp-6* as well
413 as for disruption of AIA function in *ctbp-1* mutants, we hypothesized that
414 misexpressed *ceh-28* or *acbp-6* might be contributing to the observed AIA
415 functional defect in *ctbp-1* mutants. If so, we expected that mutations that
416 eliminated the functions of these ectopically expressed genes should restore AIA
417 function in *ctbp-1* mutants. To test this hypothesis, we crossed mutant alleles of
418 *ceh-28 (cu11)* or *acbp-6 (tm2995)* (both deletion alleles spanning greater than
419 half their respective genes) to *ctbp-1(n4784)* mutants and assayed the resulting
420 double mutants for butanone adaptation in L1 and L4 worms. We found that
421 *acbp-6; ctbp-1* double mutants were nearly identical to both naïve and
422 conditioned *ctbp-1* single mutants at both the L1 and L4 larval stages (Fig. 7E-H),
423 indicating that misexpressed *acbp-6* is likely not responsible for the observed AIA
424 functional defect. Conditioned *ctbp-1 ceh-28* double mutants appeared similar to
425 both the wild type and *ctbp-1* single mutants at the L1 stage (Fig. 7I-J). These

426 double mutants display an minor, though not statistically significant, difference in
427 adaptation at the L4 larval stage when compared to either wild-type or *ctbp-1*
428 animals (Fig. 7K-L). We speculate that overexpression of *ceh-28,* caused by a
429 loss of *ctbp-1* and likely driven by ectopic *egl-13* activity, might partially account
430 for the defect in butanone adaptation seen in L4 and day 1 adult *ctbp-1* mutants
431 and that removal of *egl-13* in part restores AIA function by eliminating *ceh-28*
432 misexpression. We propose that *ctbp-1* functions to maintain aspects of the AIA
433 cell identity by preventing *egl-13* from promoting *ceh-28* expression and that *ceh-*
434 *28* misexpression can perturb proper AIA function. These results also indicate
435 that *ceh-28* overexpression alone is not solely responsible for the observed AIA
436 functional defect, suggesting that the regulation of other, as-of-yet unidentified
437 genes controlled by *ctbp-1* (and potentially *egl-13*) also contribute to the
438 maintenance of the AIA cell identity.

Discussion

We have shown that the *ctbp-1* transcriptional corepressor gene is required to maintain AIA cell identity and that *ctbp-1* negatively and selectively regulates the function of the *egl-13* transcription factor gene. We suggest that the CTBP-1 protein functions as a transcriptional corepressor to selectively regulate the transcriptional output (either directly or indirectly) of the EGL-13 protein. c*tbp-1* mutant AIAs undergo a progressive decline in their initially wild-type gene-expression pattern, morphology and function. *ctbp-1* can act cell-autonomously and is able to act in older animals to maintain these aspects of the AIA identity. We conclude that CTBP-1 functions to maintain AIA cell identity and speculate that other transcriptional corepressors similarly function in the maintenance of specific cell identities and do so by silencing undesired gene expression through repression of transcriptional activators, such as EGL-13. Such a mechanism could explain how the breadth of transcriptional activation by terminal selectors can be fine-tuned in a coordinated fashion to fit the requirements of specific cell types, with selective transcriptional silencing providing a crucial aspect of proper cell-identity maintenance.

CTBP-1 might physically interact with EGL-13 to maintain the AIA cell identity

The mammalian CtBPs (CtBP1 and CtBP2) bind PXDLS-like motifs on a number of diverse transcription factors to target specific genetic loci for silencing [49–51]. The mammalian ortholog of EGL-13, SOX6, interacts with the

462 mammalian ortholog of CTBP-1, CtBP2, through a PLNLS motif located in SOX6
463 to repress *Fgf-3* expression in the developing mouse auditory otic vesicle [74].
464 This motif is 100% conserved in *C. elegans* EGL-13. We speculate that CTBP-1
465 interacts with EGL-13 through its PLNLS motif to regulate EGL-13 activity as part
466 of AIA cell-identity maintenance. Specifically, we propose (Fig. 8) that CTBP-1
467 physically interacts with EGL-13 to target specific genetic loci for silencing as an
468 aspect of normal AIA cell-identity maintenance. Following the establishment of
469 the AIA cell fate, for which CTBP-1 is not required, CTBP-1 binds EGL-13,
470 recruiting CTBP-1 to EGL-13 DNA binding sites. CTBP-1 then silences
471 surrounding genetic loci, resulting in the repression of specific target genes (Fig.
472 8B). This repression is necessary for proper maintenance of the AIA cell identity,
473 and when disrupted, as in *ctbp-1* mutants, CTBP-1 binding partners, such as
474 EGL-13, inappropriately act as transcriptional activators in the AIAs, resulting in
475 disruption of AIA gene expression, morphology and function (Fig. 8C). In the
476 absence of such CTBP-1 interactors, as in *egl-13 ctbp-1* double mutants,
477 aberrant transcription is not activated and some of the defects in AIA
478 maintenance are avoided (Fig. 8D).
479

480 **CTBP-1 likely utilizes additional transcription factors besides EGL-13 to**
481 **maintain the AIA cell identity**

482 Our understanding of how CTBP-1 acts to maintain the AIA cell identity is
483 incomplete. While we have identified a few genes with expression that changes
484 in the absence of *ctbp-1* (*ceh-28*, *acbp-6*, *sra-11*, *glr-2*), none of these genes

485 seems to individually account for the full range of AIA defects seen in older *ctbp-*
486 *1* mutants. We speculate that there are many more unidentified transcriptional
487 changes occurring in *ctbp-1* mutant AIAs that contribute to the observed AIA
488 morphological and functional defects.

489 Our observations suggest that EGL-13 is not the sole transcription factor
490 through which CTBP-1 functions to maintain AIA cell identity – neither AIA
491 morphological defects nor some AIA gene-expression defects (i.e. *sra-11* and *glr-*
492 *2* expression) in *ctbp-1* mutants were suppressed in *egl-13 ctbp-1* double
493 mutants (Figs. 6D-G; 7A-B). We propose that CTBP-1 maintains different
494 aspects of AIA cell identity through interactions with multiple different
495 transcription factors. Given CTBP-1's known function as a transcriptional
496 corepressor and EGL-13's observed role in driving gene misexpression in the
497 absence of *ctbp-1*, we speculate that CTBP-1 likely utilizes not just EGL-13 but
498 also other transcription factors (possibly through interacting with PXDLS-like
499 motifs located in those transcription factors) to target multiple specific DNA
500 sequences for transcriptional silencing, effectively turning these transcription
501 factors into transcriptional repressors. When *ctbp-1* is absent, these unregulated
502 transcription factors can aberrantly function as transcriptional activators, resulting
503 in either the direct or indirect expression of genes which can in turn lead to
504 defects in other aspects of cell identity. Such a mechanism for the selective and
505 continuous silencing of multiple genetic loci in cell-type specific contexts by a
506 transcriptional corepressor like CTBP-1 might explain how the broad activating

507 activities of terminal selectors are restricted in the context of maintaining the
508 identities of distinct cell types.
509
510 **CTBP-1 likely maintains the identities of other cells besides that of the AIAs**
511 Others have previously reported a near pan-neuronal expression pattern
512 of *ctbp-1* in *C. elegans* [53], suggesting that *ctbp-1* might be acting in more cells
513 than just the AIAs to maintain cell identities. Why then have we thus far only
514 been able to identify defects in the maintenance of the AIA identity in *ctbp-1*
515 mutants? We speculate that, like the relatively subtle defects we have observed
516 in AIA gene expression, morphology and function, *ctbp-1* mutant defects in the
517 maintenance of other cell identities might be similarly subtle and easily missed if
518 not specifically sought. In addition, the AIAs might be particularly susceptible to
519 perturbations of maintenance of their identity, with defects manifesting either
520 earlier in the life of the cell or in more distinct ways (e.g. more gene
521 misexpression).
522 Both our findings and the work of others [54,55] provide further support for
523 the hypothesis that *ctbp-1* maintains other cell identities besides that of the AIAs.
524 We observed that *ctbp-1* mutants have an additional AIA-independent
525 chemotaxis defect (Figs. 4B-E; S5A-B), suggesting that other cells, likely neurons
526 that sense and/or execute responses to volatile odors, are also dysfunctional.
527 Additionally, others have shown that, in *ctbp-1* mutants another pair of *C.*
528 *elegans* neurons, the SMDDs, display late-onset morphological abnormalities
529 coupled with a defect in *C. elegans* foraging behavior associated with these cells

530 [54,55], indicating that CTBP-1 might act to maintain SMDD cell identity as well.
531 The broad expression of *ctbp-1* throughout much of the *C. elegans* nervous
532 system is also consistent with the hypothesis that *ctbp-1* functions broadly to
533 maintain multiple neuronal cell identities [53].
534

535 **Transcriptional corepressors might function broadly in the maintenance of**
536 **cell identities**

537 The neuron-specific expression of *ctbp-1* [53] suggests that CTBP-1 likely
538 does not function in maintaining the identities of non-neuronal cells. How might
539 non-neuronal cell identities be maintained? We speculate that transcriptional
540 corepressors function in maintaining cell identities in both neuronal and non-
541 neuronal cells. There are known tissue-specific activities of other corepressor
542 complexes, such as those of NCoR1 in mediating the downstream effects of
543 hormone sensation in the mammalian liver [75,76] or of Transducin-Like
544 Enhancer of Split (TLE) in regulating gene expression and chromatin state in the
545 developing mouse heart and kidney [77–79]. We propose that, by analogy to
546 CTBP-1, distinct transcriptional corepressors might specialize in the maintenance
547 of a wide range of cell identities in distinct tissue types throughout metazoa.

548 ## Materials and Methods

549 ### *C. elegans* strains and transgenes

550 All *C. elegans* strains were grown on Nematode Growth Medium (NGM) plates
551 seeded with *E. coli* OP50 as described previously [80]. We used the N2 Bristol
552 strain as wild type. Worms were grown at 20°C unless otherwise indicated.
553 Standard molecular biology and microinjection methods, as previously described
554 [81], were used to generate transgenic worms.

555

556 The following strains were used in this study:

Strain	Genotype
N2	wild type
MT15670	*nIs175[P_{ceh-28}::gfp]*
MT15672	*nIs177[P_{ceh-28}::gfp]*
MT15677	*nIs175; ctbp-1(n4778)*
MT16225	*nIs175; ctbp-1(n4784)*
MT15688	*nIs175; ctbp-1(n4789)*
MT15801	*nIs175; ctbp-1(n4800)*
MT15805	*nIs175; ctbp-1(n4804)*
MT15806	*nIs175; ctbp-1(n4805)*
MT15809	*nIs175; ctbp-1(n4808)*
MT15811	*nIs175; ctbp-1(n4810)*
MT15813	*nIs175; ctbp-1(n4813)*
MT15820	*nIs175; ctbp-1(n4819)*
MT15824	*nIs175; ctbp-1(n4823)*
MT15825	*nIs175; ctbp-1(n4824)*
MT15841	*nIs177; ctbp-1(n4840)*
MT15850	*nIs177; ctbp-1(n4849)*
MT15853	*nIs177; ctbp-1(n4852)*
MT15862	*nIs177; ctbp-1(n4861)*
MT15865	*nIs177; ctbp-1(n4864)*
MT15866	*nIs177; ctbp-1(n4865)*
MT26446	*nIs175; ctbp-1(tm5512)*
MT15918	*nIs175* introgressed into CB4856 “Hawaiian” background
MT16295	*nIs177* introgressed into CB4856 background
MT26522	*nIs175; ctbp-1(n4784)* introgressed into CB4856 background
MT23360	*nIs175; ctbp-1(n4784); nEx2346[ctbp-1(+)]*

MT23361	*nIs175; ctbp-1(n4784); nEx2347[ctbp-1(+)]*
MT23714	*nIs175; ctbp-1(n4784); nIs743[$P_{gcy\text{-}28.d}$::ctbp-1(+)]*
MT25271	*nIs843[$P_{gcy\text{-}28.d}$::mCherry]*
MT26437	*nIs175; ctbp-1(n4784); nIs843*
MT23365	*nIs175; ctbp-1(n4784); nEx2351[$P_{hsp\text{-}16.2}$::ctbp-1(+);$P_{hsp\text{-}16.41}$::ctbp-1(+)]*
MT18778	*nIs348[$P_{ceh\text{-}28}$::mCherry]; lin-15AB(n765ts)*
MT20844	*nIs348[$P_{ceh\text{-}28}$::mCherry]; ctbp-1(n4784)*
NH2466	*ayIs4[$P_{egl\text{-}17}$::gfp]; dpy-20(e1282ts)*
MT26417	*ayIs4; nIs348; ctbp-1(n4784)*
BW1946	*ctIs43[$P_{dbl\text{-}1}$::gfp] unc-42(e270)*
MT23726	*nIs348; ctIs43 unc-42(e270); ctbp-1(n4784)*
MT20852	*nIs491[$P_{ser\text{-}7.b}$::mCherry]*
MT23427	*nIs491; ctbp-1(n4784)*
NY2080	*ynIs80[$P_{flp\text{-}21}$::gfp]*
MT23718	*nIs348; ctbp-1(n4784); ynIs80*
OH10237	*otIs326[$P_{ins\text{-}1}$::gfp]*
MT26422	*ctbp-1(n4784); otIs326*
JN1716	*peIs1716[$P_{ins\text{-}1s}$::gfp;$P_{ttx\text{-}3}$::mCherry]*
MT23717	*nIs348; ctbp-1(n4784); peIs1716*
OH11030	*otIs317[$P_{mgl\text{-}1}$::mCherry]; otIs379[$P_{cho\text{-}1}$::gfp]*
MT26421	*nIs348; ctbp-1(n4784); otIs317; otIs379*
MT26420	*ctbp-1(n4784); otIs317*
MT25268	*nIs840[$P_{gcy\text{-}28.d}$::gfp]*
MT25270	*nIs842[$P_{gcy\text{-}28.d}$::gfp]*
MT26412	*nIs348; ctbp-1(n4784); nIs840*
MT26438	*nIs348; ctbp-1(n4784); nIs743; nIs840*
MT26439	*nIs348; ctbp-1(n4784); nIs840; nEx2351*
JN580	*peIs580[$P_{ins\text{-}1s}$::casp1;$P_{ins\text{-}1s}$::venus;$P_{unc\text{-}122}$::gfp]*
MT23746	*nIs175; egl-13(n5937) ctbp-1(n4784)*
MT24129	*nIs175; egl-13(n6013) ctbp-1(n4784)*
MT25352	*nIs175; egl-13(n6313) ctbp-1(n4784)*
MT26486	*nIs175; egl-13(n5937) ctbp-1(n4784); nEx3062[egl-13(+)]*
MT26487	*nIs175; egl-13(n5937) ctbp-1(n4784); nEx3063[egl-13(+)]*
MT26549	*nIs175; egl-13(n6013) ctbp-1(n4784); nEx3080[egl-13(+)]*
MT26523	*nIs175; egl-13(n6313) ctbp-1(n4784); nEx3074[egl-13(+)]*
MT26548	*nIs175; egl-13(n6313) ctbp-1(n4784); nEx3079[egl-13(+)]*
MT26481	*nIs175; egl-13(n5937) ctbp-1(n4784); nEx3055[$P_{gcy\text{-}28.d}$::egl-13(+)]*
MT26441	*nIs175; egl-13(n5937) ctbp-1(n4784); nIs840*
MT26415	*evIs111[$P_{rgef\text{-}1}$::gfp]; nIs843*
MT26416	*ctbp-1(n4784); evIs111; nIs843*
MT26444	*otIs123[$P_{sra\text{-}11}$::gfp]; nIs843*
MT26445	*nIs348; ctbp-1(n4784); otIs123*
MT26524	*nIs348; egl-13(n5937) ctbp-1(n4784); otIs123*
MT26504	*nIs843; ivEx138[$P_{glr\text{-}2}$::gfp]*

MT26505	*nIs348; ctbp-1(n4784); ivEx138*
MT26550	*nIs348; egl-13(n5937) ctbp-1(n4784); ivEx138*
MT26581	*nIs843; nEx3081[P_{acbp-6}::gfp]*
MT26551	*nIs348; ctbp-1(n4784); nEx3081*
MT26582	*nIs348; egl-13(n5937) ctbp-1(n4784); nEx3081*
MT26605	*acbp-6(tm2995); nIs175; ctbp-1(n4784)*
MT23725	*nIs175; ctbp-1(n4784) ceh-28(cu11)*

557

558 **Plasmid construction**

559 The *nIs175[P_{ceh-28}::gfp]*, *nIs177[P_{ceh-28}::gfp]* and *nIs348[P_{ceh-28}::mCherry]*
560 transgenes have been previously described [59]. *nIs743[$P_{gcy-28.d}$::ctbp-1(+)]*
561 contains 3.0 kb of the 5' promoter of *gcy-28.d* fused to the *ctbp-1a* coding region
562 inserted into plasmid pPD49.26. *nIs840[$P_{gcy-28.d}$::gfp]* contains 3.0 kb of the 5'
563 promoter of *gcy-28.d* inserted into pPD95.77. *nIs843[$P_{gcy-28.d}$::mCherry]* contains
564 3.0 kb of the 5' promoter of *gcy-28.d* inserted into pPD122.56 containing
565 mCherry. *nEx2351[$P_{hsp-16.2}$::ctbp-1(+);$P_{hsp-16.41}$::ctbp-1(+)]* contains *ctbp-1a*
566 cDNA, isolated by RT-PCR, inserted into pPD49.73 and pPD49.83.
567 *nEx3055[$P_{gcy-28.d}$::egl-13(+)]* contains 3.0 kb of the 5' promoter of *gcy-28.d* fused
568 to the *egl-13* coding region inserted into pPD49.26. *nEx3081[P_{acbp-6}::gfp]*
569 contains 2.0 kb of the 5' promoter of *acbp-6* inserted into pPD122.56. Plasmid
570 construction was performed using Infusion cloning enzymes (Takara Bio,
571 Mountain View, CA).

572

573 **Mutagenesis screens**

574 *ctbp-1* mutants were isolated from genetic screens for mutations that cause the
575 survival of the M4 sister cell as scored by extra GFP-positive cells carrying the
576 M4-cell-specific markers *nIs175[P_{ceh-28}::gfp]* or *nIs177[P_{ceh-28}::gfp]* [58,59]. *egl-13*

577 mutants were isolated from genetic screens for mutations that suppress *nIs175*
578 misexpression in the AIAs of *ctbp-1(n4784)* mutants while retaining GFP
579 expression in the M4 neuron. For both screens, mutagenesis was performed with
580 ethyl methanesulfonate (EMS) as previously described [80]. Mutagenized P_0
581 animals were allowed to propagate, and their F_2 progeny were synchronized by
582 hypochlorite treatment and screened at the L4 stage for extra GFP-positive cells
583 (*ctbp-1* screens) or fewer GFP-positive cells (suppressor screens) on a
584 dissecting microscope equipped to examine fluorescence. From both screens,
585 mutant alleles were grouped into functional groups by complementation testing
586 when possible. Mutants were mapped using SNP mapping [70] by crossing
587 mutants to strains containing *nIs175*, *nIs177*, or *nIs175;ctbp-1(n4784)*
588 introgressed into the Hawaiian strain CB4856. Whole-genome sequencing was
589 performed on mutants and a combination of functional groupings and mapping
590 data suggested genes with mutations that were likely causal for the mutant
591 phenotypes. Rescue of mutant phenotypes with wild-type *ctbp-1(+)* and *egl-13(+)*
592 constructs as well as the mutant phenotype of a separately isolated deletion
593 allele of *ctbp-1, tm5512,* confirmed the identities of the causal mutations.
594
595 **Microscopy**
596 All images were obtained using an LSM 800 confocal microscope (Zeiss) and
597 ZEN software. Images were processed and prepared for publication using FIJI
598 software and Adobe Illustrator.
599

600 **Heat-shock assays**

601 Rescue of AIA defects in day 1 adult worms was assayed using the
602 *nEx2351[*$P_{hsp\text{-}16.2}$*::ctbp-1;*$P_{hsp\text{-}16.41}$*::ctbp-1]* transgene. Worms were synchronized
603 and grown at 20°C. Subsets of L1 and L4 worms carrying *nEx2351* were
604 removed from this population for scoring at the appropriate stages. At the L4
605 stage, half of the worms were heat-shocked at 34°C for 30 minutes and returned
606 to 20°C for 24 hours while the other half remained at 20°C throughout. After 24
607 hours, heat-shocked and non-heat-shocked worms carrying *nEx2351* were
608 scored.

609

610 **Single-cell RNA-sequencing**

611 **Dissociation of animals into cell suspensions.** Single-cell suspensions were
612 generated as described [82–84] with minor modifications. Briefly, synchronized
613 populations of worms were grown on NGM plates seeded with OP50 to the L4
614 larval stage. Worms were harvested from these plates, washed three times with
615 M9 buffer and treated with SDS-DTT (200 mM DTT, 0.25% SDS, 20 mM HEPES,
616 3% sucrose, pH 8.0) for two to three minutes. Worms were washed five times
617 with 1x PBS and treated with pronase (15 mg/mL) for 20-23 minutes. During the
618 pronase treatment, worm suspensions were pipetted with a P200 pipette rapidly
619 for four sets of 80 repetitions. The pronase treatment was stopped by the
620 addition of L-15-10 media (90% L-15 media, 10% FBS). The suspension was
621 then passed through a 35 μm nylon filter into a collection tube, washed once with
622 1x PBS, and prepared for FACS.

623

624 **FACS of fluorescently-labeled neurons.** FACS was performed using a BD
625 FACSAria III cell sorter running BD FACS Diva software. DAPI was added to
626 samples at a final concentration of 1 µg/mL to label dead and dying cells. GFP-
627 positive, DAPI-negative neurons were sorted from the single-cell suspension into
628 1x PBS containing 1% FBS. Non-fluorescent and single-color controls were used
629 to set gating parameters. Cells were then concentrated and processed for single-
630 cell sequencing.

631

632 **Single-cell sequencing.** Samples were processed for single-cell sequencing
633 using the 10X Genomics Chromium 3'mRNA-sequencing platform. Libraries were
634 prepared using the Chromium Next GEM Single Cell 3' Kit v3.1 according to the
635 manufacturer's protocol. The libraries were sequenced using an Illumina
636 NextSeq 500 with 75 bp paired end reads.

637

638 **Single-cell RNA-sequencing data processing.** Data processing was performed
639 using 10X Genomics' CellRanger software (v4.0.0). Reads were mapped to the
640 *C. elegans* reference genome from Wormbase, version WBcel235. For
641 visualization and analysis of data, we used 10X Genomics' Loupe Browser
642 (v4.2.0). AIAs were identified by expression of multiple AIA markers confirmed to
643 be expressed in both wild-type and *ctbp-1* mutant AIAs (i.e. *gcy-28, ins-1, cho-1*;
644 Fig. 2B). Candidate genes for misexpression (either ectopic or missing) in mutant
645 AIAs were identified and tested as described in the text.

646

647 **Morphology scoring**

648 We assayed AIA morphology by visualizing and imaging AIAs expressing *nIs840*
649 using an LSM 800 confocal microscope (Zeiss) and a 63x objective. AIA cell
650 body length and area were quantified using FIJI software.

651

652 **Image blinding and scoring**

653 A subset of 60 wild-type and 60 *ctbp-1* mutant images per stage (randomly
654 chosen from the existing images taken to measure AIA cell body length) were
655 selected and the genotype of each was blinded. Blinded images were then
656 scored as either “Normal” or “Elongated” in appearance in batches of 40 images
657 (20 each of wild-type and *ctbp-1* mutant, randomly assorted), repeated three
658 times per stage. Scored images were then matched back to their genotypes and
659 percentage of AIAs scored as “Elongated” per genotype was calculated and
660 graphed.

661

662 **Behavioral Assays**

663 **Butanone adaptation.** Assay conditions were adapted from Cho et al., 2016
664 [66]. Staged worms were washed off non-crowded NGM plates seeded with *E.*
665 *coli* OP50 with S basal. Worms were washed two times with S basal and split
666 evenly into the “naïve” and “conditioned” populations. Naïve worms were
667 incubated in 1 mL S basal for 90 minutes. Conditioned worms were incubated in
668 1 mL S basal with 2-butanone diluted to a final concentration of 120 μM for 90

669 minutes. During conditioning, unseeded NGM plates were spotted with two 1 μL
670 drops of 10% ethanol ("control") and two 1 μL drops of 2-butanone diluted in 10%
671 ethanol at 1:1000 ("odor") as well as four 1 μL drops of 1 M NaN_3 at the same
672 loci. After conditioning, both populations were washed three more times in S
673 basal and placed at the center of the unseeded NGM plates. Worms were
674 allowed to chemotax for two hours. Plates were moved to 4°C for 30-60 minutes
675 to stop the assay and then scored. Worms that had left the origin were scored as
676 chemotaxing to the odor spots ("#odor") or control spots ("#control"), and a
677 chemotaxis index was determined as (#odor - #control) / (#odor + #control).
678 Assays were repeated on at least three separate days with one to three plates
679 per strain ran in parallel on any given day based on the number of appropriately-
680 staged worms available. Plates in which fewer than 50 worms left the origin were
681 not scored.
682
683 **Chemotaxis assays.** L4 worms were washed off non-crowded NGM plates
684 seeded with *E. coli* OP50 with S basal. Worms were washed three times with S
685 basal. Unseeded NGM plates were spotted with two 1 μL drops of 100% ethanol
686 ("control") and two 1 μL drops of diacetyl diluted in 100% ethanol at 1:1000 or
687 two 1 μL drops of isoamyl alcohol diluted in 100% ethanol at 1:100 ("odor") as
688 well as four 1 μL drops of 1 M NaN_3 at the same loci. Worms were placed at the
689 center of the unseeded NGM plates. Worms were allowed to chemotax for two
690 hours. Plates were moved to 4°C for 30-60 minutes to stop the assay and then
691 scored. Worms that had left the origin were scored, and a chemotaxis index was

692 determined as above. Assays were repeated on at least three separate days.

693 Plates in which fewer than 40 worms left the origin were not scored.

694

695 **Statistical analyses**

696 Unpaired t-tests were used for the comparisons of AIA gene expression and AIA

697 morphological features. One-way ANOVA tests with Tukey's correction were

698 used for comparisons of AIA morphological features and for behavioral assays.

699 Statistical tests were performed using GraphPad Prism software (GraphPad

700 Prism version 6.0h, RRID: SCR_002798).

701

702 **Accession Number**

703 The GEO accession number for the RNA-Seq dataset in this paper is

704 GSE179484.

Acknowledgments

We thank N. An, R. Droste, S. Mitani, and the *Caenorhabditis* Genetics Center (CGC), which is funded by NIH Office of Research Infrastructure Programs (P40 OD010440), for strains and reagents. We thank C. Diehl, E. Lee, C. Pender, S. Sando, V. Dwivedi, K. Burkhart, S. Wong, C. Fincher, C. Cho, G. Johnson, D. Lee, D. Ghosh, A. Amon, P. Reddien, and Horvitz laboratory members for discussion and advice.

Funding

National Institutes of Health (GM024663)

- Josh Saul
- H. Robert Horvitz

National Institutes of Health (T32GM007287)

- Josh Saul

Howard Hughes Medical Institute

- Josh Saul
- Takashi Hirose
- H. Robert Horvitz

Friends of the McGovern Institute Fellowship (2733360)

- Josh Saul

Author Contributions

H.R.H. supervised the project. T.H. initiated the project. J.S. and T.H. designed and performed experiments, generated reagents, and analyzed data. All authors contributed to interpretation of data. J.S. wrote the original manuscript draft. All authors contributed to review and editing of the manuscript.

Declaration of Interests

The authors declare no competing interests.

734 ## References

735 1. Davidson EH, Cameron RA, Ransick A. Specification of cell fate in the sea
736 urchin embryo: summary and some proposed mechanisms. Dev Camb Engl.
737 1998 Sep;125(17):3269–90.
738 2. Davidson EH. A Genomic Regulatory Network for Development. Science.
739 2002 Mar 1;295(5560):1669–78.
740 3. Levine M, Davidson EH. Gene regulatory networks for development. Proc
741 Natl Acad Sci. 2005 Apr 5;102(14):4936–42.
742 4. Hobert O. A map of terminal regulators of neuronal identity in
743 Caenorhabditis elegans. Wiley Interdiscip Rev Dev Biol. 5(4):474–98.
744 5. Hsieh J, Zhao X. Genetics and Epigenetics in Adult Neurogenesis. Cold
745 Spring Harb Perspect Biol [Internet]. 2016 Jun [cited 2021 Mar 18];8(6).
746 Available from: https://www.ncbi.nlm.nih.gov/pmc/articles/PMC4888816/
747 6. Homem CCF, Repic M, Knoblich JA. Proliferation control in neural stem and
748 progenitor cells. Nat Rev Neurosci. 2015 Nov;16(11):647–59.
749 7. Altun-Gultekin Z, Andachi Y, Tsalik EL, Pilgrim D, Kohara Y, Hobert O. A
750 regulatory cascade of three homeobox genes, ceh-10, ttx-3 and ceh-23,
751 controls cell fate specification of a defined interneuron class in C. elegans.
752 Development. 2001 Jun 1;128(11):1951–69.
753 8. Zeng H, Sanes JR. Neuronal cell-type classification: challenges,
754 opportunities and the path forward. Nat Rev Neurosci. 2017 Sep;18(9):530–
755 46.

9. Baker NE. Master regulatory genes; telling them what to do. BioEssays. 2001;23(9):763–6.
10. Deneris ES, Hobert O. Maintenance of postmitotic neuronal cell identity. Nat Neurosci. 2014 Jul;17(7):899–907.
11. Hobert O, Carrera I, Stefanakis N. The molecular and gene regulatory signature of a neuron. Trends Neurosci. 2010 Oct 1;33(10):435–45.
12. Masoudi N, Tavazoie S, Glenwinkel L, Ryu L, Kim K, Hobert O. Unconventional function of an Achaete-Scute homolog as a terminal selector of nociceptive neuron identity. PLOS Biol. 2018 Apr 19;16(4):e2004979.
13. Weintraub H, Dwarki VJ, Verma I, Davis R, Hollenberg S, Snider L, et al. Muscle-specific transcriptional activation by MyoD. Genes Dev. 1991 Aug 1;5(8):1377–86.
14. Lassar AB. Finding MyoD and lessons learned along the way. Semin Cell Dev Biol. 2017 Dec;72:3–9.
15. Wardle FC. Master control: transcriptional regulation of mammalian Myod. J Muscle Res Cell Motil. 2019 Jun;40(2):211–26.
16. Halder G, Callaerts P, Gehring WJ. Induction of ectopic eyes by targeted expression of the eyeless gene in Drosophila. Science. 1995 Mar 24;267(5205):1788–92.
17. Gehring WJ. The master control gene for morphogenesis and evolution of the eye. Genes Cells. 1996;1(1):11–5.

778 18. Shen W, Mardon G. Ectopic eye development in Drosophila induced by
779 directed dachshund expression. Dev Camb Engl. 1997 Jan;124(1):45–52.
780 19. Treisman JE. Retinal differentiation in Drosophila. WIREs Dev Biol.
781 2013;2(4):545–57.
782 20. Lima Cunha D, Arno G, Corton M, Moosajee M. The Spectrum of PAX6
783 Mutations and Genotype-Phenotype Correlations in the Eye. Genes. 2019
784 Dec;10(12):1050.
785 21. Fukushige T, Hawkins MG, McGhee JD. The GATA-factor elt-2 is essential
786 for formation of the Caenorhabditis elegans intestine. Dev Biol. 1998 Jun
787 15;198(2):286–302.
788 22. Fukushige T, Hendzel MJ, Bazett-Jones DP, McGhee JD. Direct
789 visualization of the elt-2 gut-specific GATA factor binding to a target
790 promoter inside the living Caenorhabditis elegans embryo. Proc Natl Acad
791 Sci. 1999 Oct 12;96(21):11883–8.
792 23. McGhee JD, Fukushige T, Krause MW, Minnema SE, Goszczynski B,
793 Gaudet J, et al. ELT-2 Is the Predominant Transcription Factor Controlling
794 Differentiation and Function of the C. elegans Intestine, from Embryo to
795 Adult. Dev Biol. 2009 Mar 15;327(2):551–65.
796 24. Block DH, Shapira M. GATA transcription factors as tissue-specific master
797 regulators for induced responses. Worm. 2015 Oct 2;4(4):e1118607.
798 25. Matson CK, Murphy MW, Sarver AL, Griswold MD, Bardwell VJ, Zarkower
799 D. DMRT1 prevents female reprogramming in the postnatal mammalian
800 testis. Nature. 2011 Aug 4;476(7358):101–4.

801 26. Mall M, Kareta MS, Chanda S, Ahlenius H, Perotti N, Zhou B, et al. Myt1l
802 safeguards neuronal identity by actively repressing many non-neuronal
803 fates. Nature [Internet]. 2017 Apr 5 [cited 2017 Apr 7];advance online
804 publication. Available from:
805 http://www.nature.com/nature/journal/vaop/ncurrent/full/nature21722.html
806 27. Simon HH, Thuret S, Alberi L. Midbrain dopaminergic neurons: control of
807 their cell fate by the engrailed transcription factors. Cell Tissue Res. 2004
808 Sep 1;318(1):53–61.
809 28. Vissers JHA, Froldi F, Schröder J, Papenfuss AT, Cheng LY, Harvey KF.
810 The Scalloped and Nerfin-1 Transcription Factors Cooperate to Maintain
811 Neuronal Cell Fate. Cell Rep. 2018 Nov 6;25(6):1561-1576.e7.
812 29. Hsiao H-Y, Jukam D, Johnston R, Desplan C. The neuronal transcription
813 factor erect wing regulates specification and maintenance of Drosophila R8
814 photoreceptor subtypes. Dev Biol. 2013 Sep 15;381(2):482–90.
815 30. Riddle MR, Weintraub A, Nguyen KCQ, Hall DH, Rothman JH.
816 Transdifferentiation and remodeling of post-embryonic C. elegans cells by a
817 single transcription factor. Development. 2013 Dec 15;140(24):4844–9.
818 31. O'Meara MM, Zhang F, Hobert O. Maintenance of Neuronal Laterality in
819 Caenorhabditis elegans Through MYST Histone Acetyltransferase Complex
820 Components LSY-12, LSY-13 and LIN-49. Genetics. 2010 Dec
821 1;186(4):1497–502.

822 32. Xu J, Hao X, Yin M-X, Lu Y, Jin Y, Xu J, et al. Prevention of medulla neuron
823 dedifferentiation by Nerfin-1 requires inhibition of Notch activity.
824 Development. 2017 Apr 15;144(8):1510–7.
825 33. Hobert O. Regulatory logic of neuronal diversity: Terminal selector genes
826 and selector motifs. Proc Natl Acad Sci. 2008 Dec 23;105(51):20067–71.
827 34. Hobert O. Regulation of Terminal Differentiation Programs in the Nervous
828 System. Annu Rev Cell Dev Biol. 2011;27(1):681–96.
829 35. Hobert O, Kratsios P. Neuronal identity control by terminal selectors in
830 worms, flies, and chordates. Curr Opin Neurobiol. 2019 Jun 1;56:97–105.
831 36. Hobert O. Terminal Selectors of Neuronal Identity. Curr Top Dev Biol.
832 2016;116:455–75.
833 37. Zhang F, Bhattacharya A, Nelson JC, Abe N, Gordon P, Lloret-Fernandez C,
834 et al. The LIM and POU homeobox genes ttx-3 and unc-86 act as terminal
835 selectors in distinct cholinergic and serotonergic neuron types.
836 Development. 2014 Jan 15;141(2):422–35.
837 38. Serrano-Saiz E, Poole RJ, Felton T, Zhang F, De La Cruz ED, Hobert O.
838 Modular Control of Glutamatergic Neuronal Identity in C. elegans by Distinct
839 Homeodomain Proteins. Cell. 2013 Oct 24;155(3):659–73.
840 39. Duggan A, Ma C, Chalfie M. Regulation of touch receptor differentiation by
841 the Caenorhabditis elegans mec-3 and unc-86 genes. Dev Camb Engl. 1998
842 Oct;125(20):4107–19.
843 40. Kim J, Yeon J, Choi S-K, Huh YH, Fang Z, Park SJ, et al. The Evolutionarily
844 Conserved LIM Homeodomain Protein LIM-4/LHX6 Specifies the Terminal

845 Identity of a Cholinergic and Peptidergic C. elegans Sensory/Inter/Motor
846 Neuron-Type. PLOS Genet. 2015 Aug 25;11(8):e1005480.
847 41. Alqadah A, Hsieh Y-W, Vidal B, Chang C, Hobert O, Chuang C-F.
848 Postmitotic diversification of olfactory neuron types is mediated by
849 differential activities of the HMG-box transcription factor SOX-2. EMBO J.
850 2015 Oct 14;34(20):2574–89.
851 42. Kerk SY, Kratsios P, Hart M, Mourao R, Hobert O. Diversification of
852 C. elegans Motor Neuron Identity via Selective Effector Gene Repression.
853 Neuron. 2017 Jan 4;93(1):80–98.
854 43. Zhou HM, Walthall WW. UNC-55, an Orphan Nuclear Hormone Receptor,
855 Orchestrates Synaptic Specificity among Two Classes of Motor Neurons in
856 Caenorhabditis elegans. J Neurosci. 1998 Dec 15;18(24):10438–44.
857 44. Winnier AR, Meir JY-J, Ross JM, Tavernarakis N, Driscoll M, Ishihara T, et
858 al. UNC-4/UNC-37-dependent repression of motor neuron-specific genes
859 controls synaptic choice in Caenorhabditis elegans. Genes Dev. 1999 Nov
860 1;13(21):2774–86.
861 45. Yu B, Wang X, Wei S, Fu T, Dzakah EE, Waqas A, et al. Convergent
862 Transcriptional Programs Regulate cAMP Levels in C. elegans GABAergic
863 Motor Neurons. Dev Cell. 2017 Oct 23;43(2):212-226.e7.
864 46. Wyler SC, Spencer WC, Green NH, Rood BD, Crawford L, Craige C, et al.
865 Pet-1 Switches Transcriptional Targets Postnatally to Regulate Maturation of
866 Serotonin Neuron Excitability. J Neurosci. 2016 Feb 3;36(5):1758–74.

867 47. Turner J, Crossley M. The CtBP family: enigmatic and enzymatic
868 transcriptional co-repressors. BioEssays. 2001 Aug 1;23(8):683–90.
869 48. Chinnadurai G. CtBP, an Unconventional Transcriptional Corepressor in
870 Development and Oncogenesis. Mol Cell. 2002 Feb;9(2):213–24.
871 49. Chinnadurai G. CtBP family proteins: More than transcriptional
872 corepressors. BioEssays. 2003 Jan 1;25(1):9–12.
873 50. Shi Y, Sawada J, Sui G, Affar EB, Whetstine JR, Lan F, et al. Coordinated
874 histone modifications mediated by a CtBP co-repressor complex. Nature.
875 2003 Apr 17;422(6933):735–8.
876 51. Stankiewicz TR, Gray JJ, Winter AN, Linseman DA. C-terminal binding
877 proteins: central players in development and disease. Biomol Concepts.
878 2014;5(6):489–511.
879 52. Nicholas HR, Lowry JA, Wu T, Crossley M. The Caenorhabditis elegans
880 Protein CTBP-1 Defines a New Group of THAP Domain-Containing CtBP
881 Corepressors. J Mol Biol. 2008 Jan 4;375(1):1–11.
882 53. Reid A, Yücel D, Wood M, Llamosas E, Kant S, Crossley M, et al. The
883 transcriptional repressor CTBP-1 functions in the nervous system of
884 Caenorhabditis elegans to regulate lifespan. Exp Gerontol. 2014
885 Dec;60:153–65.
886 54. Reid A, Sherry TJ, Yücel D, Llamosas E, Nicholas HR. The C-terminal
887 binding protein (CTBP-1) regulates dorsal SMD axonal morphology in
888 Caenorhabditis elegans. Neuroscience. 2015 Dec 17;311:216–30.

889 55. Sherry T, Handley A, Nicholas HR, Pocock R. Harmonization of L1CAM
890 expression facilitates axon outgrowth and guidance of a motor neuron.
891 Development [Internet]. 2020 Jan 1 [cited 2020 Oct 8]; Available from:
892 https://dev.biologists.org/content/early/2020/10/07/dev.193805
893 56. Petersen JG, Romanos TR, Juozaityte V, Riveiro AR, Hums I, Traunmüller
894 L, et al. EGL-13/SoxD Specifies Distinct O2 and CO2 Sensory Neuron Fates
895 in Caenorhabditis elegans. PLOS Genet. 2013 May 9;9(5):e1003511.
896 57. Cinar HN, Richards KL, Oommen KS, Newman AP. The EGL-13 SOX
897 domain transcription factor affects the uterine pi cell lineages in
898 Caenorhabditis elegans. Genetics. 2003 Nov;165(3):1623–8.
899 58. Hirose T, Horvitz HR. An Sp1 transcription factor coordinates caspase-
900 dependent and -independent apoptotic pathways. Nature. 2013
901 Aug;500(7462):354–8.
902 59. Hirose T, Galvin BD, Horvitz HR. Six and Eya promote apoptosis through
903 direct transcriptional activation of the proapoptotic BH3-only gene egl-1 in
904 Caenorhabditis elegans. Proc Natl Acad Sci. 2010 Aug 31;107(35):15479–
905 84.
906 60. C. elegans Deletion Mutant Consortium. large-scale screening for targeted
907 knockouts in the Caenorhabditis elegans genome. G3 Bethesda Md. 2012
908 Nov;2(11):1415–25.
909 61. Ramakrishnan K, Okkema PG. Regulation of C. elegans Neuronal
910 Differentiation by the ZEB-Family Factor ZAG-1 and the NK-2
911 Homeodomain Factor CEH-28. PLOS ONE. 2014 Dec 4;9(12):e113893.

912 62. Ramakrishnan K, Ray P, Okkema PG. CEH-28 activates dbl-1 expression
913 and TGF-β signaling in the C. elegans M4 neuron. Dev Biol. 2014 Jun
914 15;390(2):149–59.
915 63. Tomioka M, Adachi T, Suzuki H, Kunitomo H, Schafer WR, Iino Y. The
916 Insulin/PI 3-Kinase Pathway Regulates Salt Chemotaxis Learning in
917 Caenorhabditis elegans. Neuron. 2006 Sep 7;51(5):613–25.
918 64. Iino Y, Yoshida K. Parallel use of two behavioral mechanisms for
919 chemotaxis in Caenorhabditis elegans. J Neurosci Off J Soc Neurosci. 2009
920 Apr 29;29(17):5370–80.
921 65. Shinkai Y, Yamamoto Y, Fujiwara M, Tabata T, Murayama T, Hirotsu T, et
922 al. Behavioral Choice between Conflicting Alternatives Is Regulated by a
923 Receptor Guanylyl Cyclase, GCY-28, and a Receptor Tyrosine Kinase,
924 SCD-2, in AIA Interneurons of Caenorhabditis elegans. J Neurosci. 2011
925 Feb 23;31(8):3007–15.
926 66. Cho CE, Brueggemann C, L'Etoile ND, Bargmann CI. Parallel encoding of
927 sensory history and behavioral preference during Caenorhabditis elegans
928 olfactory learning. eLife. 2016 Jul 6;5:e14000.
929 67. Shaye DD, Greenwald I. OrthoList: A Compendium of C. elegans Genes
930 with Human Orthologs. PLOS ONE. 2011 May 25;6(5):e20085.
931 68. Troemel ER, Chou JH, Dwyer ND, Colbert HA, Bargmann CI. Divergent
932 seven transmembrane receptors are candidate chemosensory receptors in
933 C. elegans. Cell. 1995 Oct 20;83(2):207–18.

934 69. Brockie PJ, Madsen DM, Zheng Y, Mellem J, Maricq AV. Differential
935 Expression of Glutamate Receptor Subunits in the Nervous System of
936 Caenorhabditis elegans and Their Regulation by the Homeodomain Protein
937 UNC-42. J Neurosci. 2001 Mar 1;21(5):1510–22.
938 70. Davis MW, Hammarlund M, Harrach T, Hullett P, Olsen S, Jorgensen EM.
939 Rapid single nucleotide polymorphism mapping in C. elegans. BMC
940 Genomics. 2005;6:118.
941 71. Feng G, Yi P, Yang Y, Chai Y, Tian D, Zhu Z, et al. Developmental stage-
942 dependent transcriptional regulatory pathways control neuroblast lineage
943 progression. Development. 2013 Sep 15;140(18):3838–47.
944 72. Ji EH, Kim J. SoxD Transcription Factors: Multifaceted Players of Neural
945 Development. Int J Stem Cells. 2016 May 30;9(1):3–8.
946 73. Saleem M, Barturen-Larrea P, Gomez JA. Emerging roles of Sox6 in the
947 renal and cardiovascular system. Physiol Rep. 2020 Nov;8(22):e14604.
948 74. Murakami A, Ishida S, Thurlow J, Revest J-M, Dickson C. SOX6 binds
949 CtBP2 to repress transcription from the Fgf-3 promoter. Nucleic Acids Res.
950 2001 Aug 15;29(16):3347–55.
951 75. Feng X, Jiang Y, Meltzer P, Yen PM. Transgenic Targeting of a Dominant
952 Negative Corepressor to Liver Blocks Basal Repression by Thyroid
953 Hormone Receptor and Increases Cell Proliferation*. J Biol Chem. 2001 Jan
954 1;276(18):15066–72.
955 76. Mottis A, Mouchiroud L, Auwerx J. Emerging roles of the corepressors
956 NCoR1 and SMRT in homeostasis. Genes Dev. 2013 Apr 15;27(8):819–35.

957 77. Sharma M, Brantley JG, Vassmer D, Chaturvedi G, Baas J, Vanden Heuvel
958 GB. The homeodomain protein Cux1 interacts with Grg4 to repress p27kip1
959 expression during kidney development. Gene. 2009 Jun 15;439(1):87–94.
960 78. Kaltenbrun E, Greco TM, Slagle CE, Kennedy LM, Li T, Cristea IM, et al. A
961 Gro/TLE-NuRD Corepressor Complex Facilitates Tbx20-Dependent
962 Transcriptional Repression. J Proteome Res. 2013 Dec 6;12(12):5395–409.
963 79. Agarwal M, Kumar P, Mathew SJ. The Groucho/Transducin-like enhancer of
964 split protein family in animal development. IUBMB Life. 2015 Jul
965 1;67(7):472–81.
966 80. Brenner S. The Genetics of CAENORHABDITIS ELEGANS. Genetics. 1974
967 May;77(1):71–94.
968 81. Mello CC, Kramer JM, Stinchcomb D, Ambros V. Efficient gene transfer in
969 C.elegans: extrachromosomal maintenance and integration of transforming
970 sequences. EMBO J. 1991 Dec;10(12):3959–70.
971 82. Taylor SR, Santpere G, Reilly M, Glenwinkel L, Poff A, McWhirter R, et al.
972 Expression profiling of the mature C. elegans nervous system by single-cell
973 RNA-Sequencing. bioRxiv. 2019 Aug 17;737577.
974 83. Kaletsky R, Lakhina V, Arey R, Williams A, Landis J, Ashraf J, et al. The C.
975 elegans adult neuronal IIS/FOXO transcriptome reveals adult phenotype
976 regulators. Nature. 2016 Jan;529(7584):92–6.
977 84. Zhang S. Cell isolation and culture. WormBook. 2013 Feb 21;1–39.
978

979 # Figures

980

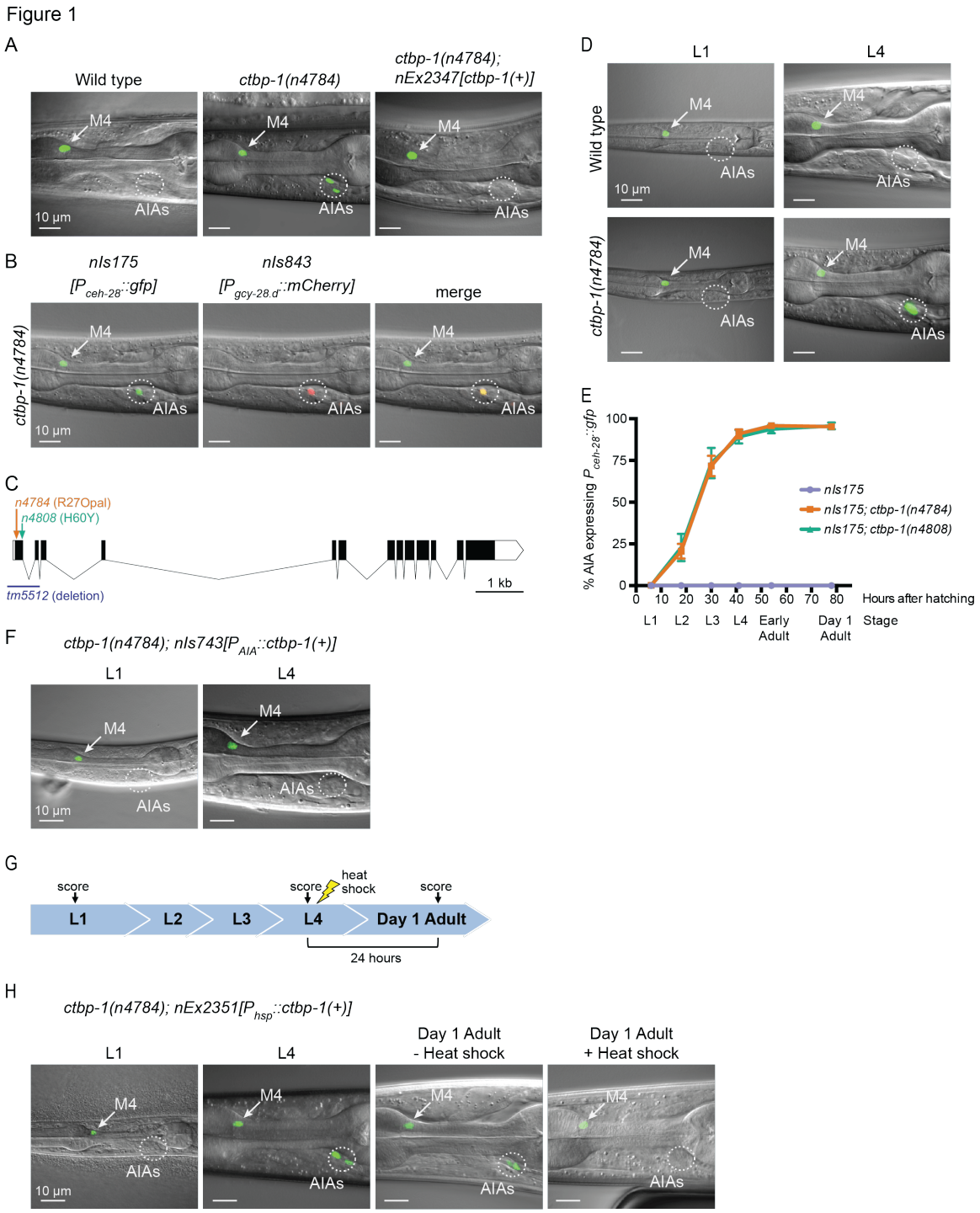

981

982 **Figure 1. *ctbp-1* mutants misexpress *P_{ceh-28}::gfp* in the AIA neurons**

983 (A) Expression of the M4-specific marker *nIs175[P_{ceh-28}::gfp]* in the wild type (left
984 panel), a *ctbp-1(n4784)* mutant (middle panel), and a *ctbp-1* mutant carrying an
985 extrachromosomal array expressing wild-type *ctbp-1* under its native promoter
986 (*nEx2347*) (right panel). Arrow, M4 neuron. Circle, AIAs. Scale bar, 10 μm.
987 (B) A *ctbp-1(n4784)* mutant expressing *nIs175* (left panel) and the AIA marker
988 *nIs843[$P_{gcy-28.d}$::mCherry]* (middle panel). Merge, right panel. Arrow, M4 neuron.
989 Circle, AIAs. Scale bar, 10 μm.
990 (C) Gene diagram of the *ctbp-1a* isoform. Arrows (above), point mutations. Line
991 (below), deletion. Scale bar (bottom right), 1 kb. Additional *ctbp-1* alleles are
992 shown in Fig. S1B.
993 (D) *nIs175* expression in wild-type (top) and *ctbp-1(n4784)* (bottom) worms at the
994 L1 larval stage (left) and L4 larval stage (right). Arrow, M4 neuron. Circle, AIAs.
995 Scale bar, 10 μm.
996 (E) Percentage of wild-type, *ctbp-1(n4784)*, and *ctbp-1(n4808)* worms expressing
997 *nIs175* in the AIA neurons over time. Time points correspond to the L1, L2, L3,
998 and L4 larval stages, early adult, and day 1 adult worms (indicated below X axis).
999 Mean ± SEM. $n \geq 60$ worms scored per strain per stage, 4 biological replicates.
1000 (F) Expression of *nIs175* in *ctbp-1* mutants containing a transgene driving
1001 expression of wild-type *ctbp-1* under an AIA-specific promoter (*nIs743[P_{gcy-}*
1002 *$_{28.d}$::ctbp-1(+)]*) in L1 and L4 larval worms. Arrow, M4 neuron. Circle, AIAs. Scale
1003 bar, 10 μm.
1004 (G) Schematic for the heat shock experiment shown in Fig. 1H.

1005 (H) *nIs175* expression in *ctbp-1(n4784)* mutants carrying the heat shock-

1006 inducible transgene *nEx2351[$P_{hsp\text{-}16.2}$::ctbp-1(+);$P_{hsp\text{-}16.41}$::ctbp-1(+)]*. Arrow, M4

1007 neuron. Circle, AIAs. Scale bar, 10 µm.

1008 All strains shown contain the transgene *nIs175[$P_{ceh\text{-}28}$::gfp].*

1009 Images are oriented such that left corresponds to anterior, top to dorsal.

1010

Figure 2

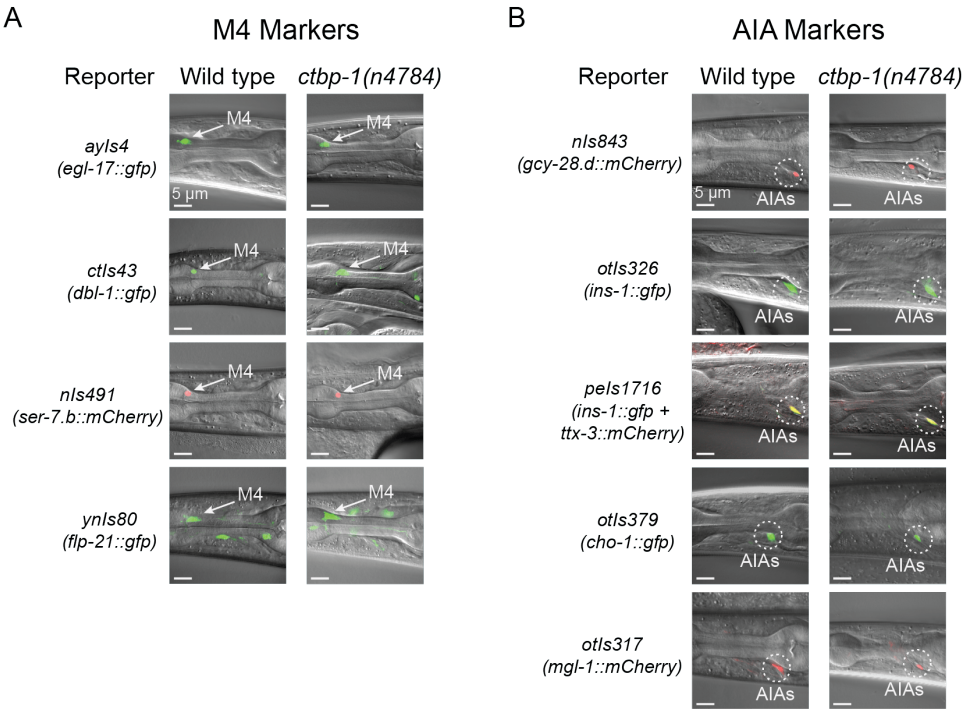

1011

1012 **Figure 2. *ctbp-1* mutant AIAs retain multiple aspects of their AIA gene**

1013 **expression profile**

1014 (A-B) Expression of (A) M4 markers *egl-17*, *dbl-1*, *ser-7.b* and *flp-21* and (B) AIA

1015 markers *gcy-28.d*, *ins-1*, *ttx-3*, *cho-1* and *mgl-1* in wild-type (left image) and *ctbp-*

1016 *1(n4784)* (right image) L4 larval worms. Arrow, M4 neuron. Circles, AIAs. Scale

1017 bar, 5 µm.

1018 Images are oriented such that left corresponds to anterior, top to dorsal.

1019

Figure 3

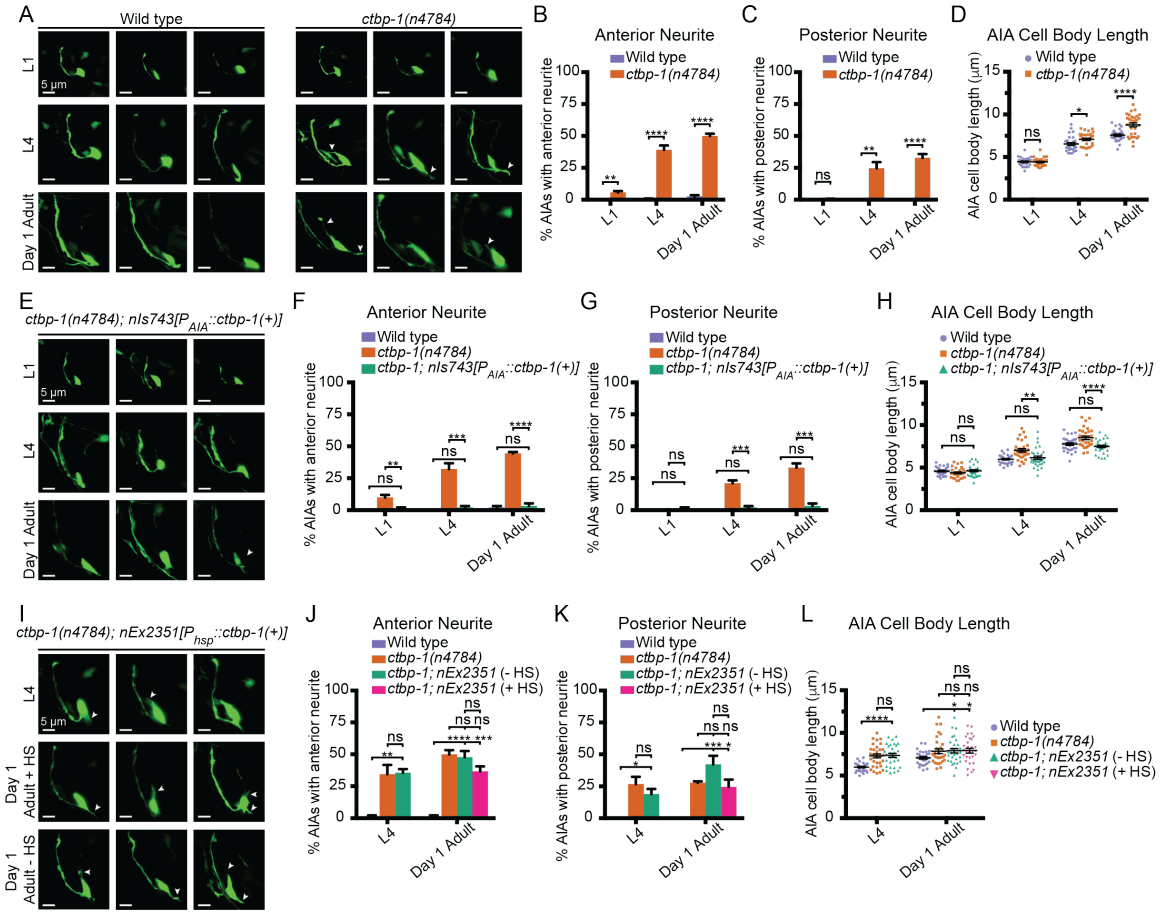

1020

1021 **Figure 3. Loss of *ctbp-1* results in a progressive decline in AIA morphology**

1022 (A) Three representative images of an AIA neuron in wild-type (left) and *ctbp-*

1023 *1(n4784)* (right) worms at L1 (top), L4 (middle) and day 1 adult (bottom) stages.

1024 Arrows, examples of ectopic neurites protruding from the AIA cell body. Scale

1025 bar, 5 µm.

1026 (B-C) Percentage of AIAs in wild-type and *ctbp-1* worms at the L1, L4 and day 1

1027 adult stages with an ectopic neurite protruding from the (B) anterior or (C)

1028 posterior of the AIA cell body. Mean ± SEM. *n* = 60 AIAs scored per strain per

1029 stage, 4 biological replicates. ns, not significant, **p<0.01, ****p<0.0001,
1030 unpaired t-test.
1031 (D) Quantification of AIA cell body length in wild-type and *ctbp-1* worms at the
1032 L1, L4 and day 1 adult stages. Mean ± SEM. *n* = 30 AIAs scored per strain per
1033 stage. ns, not significant, *p<0.05, ****p<0.0001, unpaired t-test.
1034 (E) Three representative images of an AIA neuron in *ctbp-1; nIs743[*P_{gcy-}
1035 $_{28.d}$*::ctbp-1(+)]* worms at L1 (top), L4 (middle) and day 1 adult (bottom) stages.
1036 Arrows, examples of ectopic neurites protruding from the AIA cell body. Scale
1037 bar, 5 µm.
1038 (F-G) Percentage of AIAs in wild-type, *ctbp-1* and *ctbp-1; nIs743* worms at the
1039 L1, L4 and day 1 adult stages with an ectopic neurite protruding from the (F)
1040 anterior or (G) posterior of the AIA cell body. Mean ± SEM. *n* = 30 AIAs scored
1041 per strain per stage, 3 biological replicates. ns, not significant, **p<0.01,
1042 ***p<0.001, ****p<0.0001, one-way ANOVA with Tukey's correction.
1043 (H) Quantification of AIA cell body length in wild-type, *ctbp-1* and *ctbp-1; nIs743*
1044 worms at the L1, L4 and day 1 adult stages. Mean ± SEM. *n* ≥ 30 AIAs scored
1045 per strain per stage. ns, not significant, **p<0.01, ****p<0.0001, one-way ANOVA
1046 with Tukey's correction.
1047 (I) Three representative images of an AIA neuron in *ctbp-1; nEx2351[*P_{hsp-}
1048 $_{16.2}$*::ctbp-1(+);*$P_{hsp-16.41}$*::ctbp-1(+)]* worms at L4 (top), day 1 adult with heat shock
1049 (HS) (middle) and day 1 adult without heat shock (bottom). Arrows, examples of
1050 ectopic neurites protruding from the AIA cell body. Scale bar, 5 µm.

1051 (J-K) Percentage of AIAs in wild-type, *ctbp-1* and *ctbp-1; nEx2351* worms at L4
1052 and day 1 adult (with or without heat shock) stages with an ectopic neurite
1053 protruding from the (J) anterior or (K) posterior of the AIA cell body. Mean ±
1054 SEM. *n* = 30 AIAs scored per strain per stage, 3 biological replicates. ns, not
1055 significant, *p<0.05, **p<0.01, ***p<0.001, ****p<0.0001, one-way ANOVA with
1056 Tukey's correction.
1057 (L) Quantification of AIA cell body length in wild-type, *ctbp-1* and *ctbp-1;*
1058 *nEx2351* worms at L4 and day 1 adult (with or without heat shock) stages. Mean
1059 ± SEM. *n* ≥ 30 AIAs scored per strain per stage. ns, not significant, *p<0.05,
1060 ****p<0.0001, one-way ANOVA with Tukey's correction.
1061 The *ctbp-1* allele used for all panels of this figure was *n4784*.
1062 All strains contain *nIs840[*$P_{gcy\text{-}28.d}$*::gfp],* and all strains other than "Wild type"
1063 contain *nIs348[*$P_{ceh\text{-}28}$*::mCherry]* (not shown in images).
1064 Images are oriented such that left corresponds to anterior, top to dorsal.
1065

Figure 4

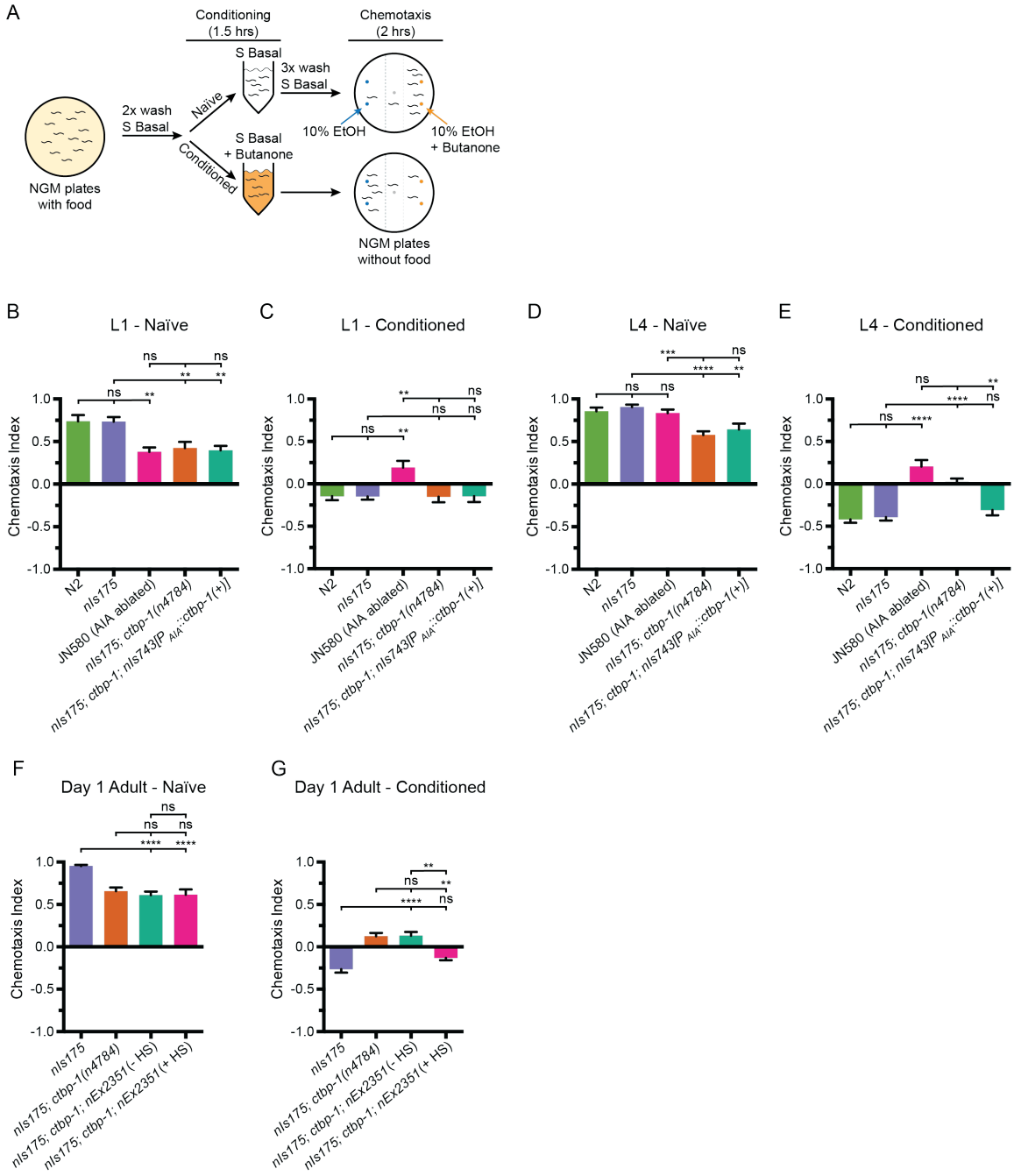

Figure 4. Loss of *ctbp-1* results in a disruption of AIA function in L4-to-day 1 adult worms

(A) Schematic of the butanone adaptation assay. L1 or L4 worms from synchronized populations were washed off plates with S Basal, washed with S

1071 Basal, split into naïve and conditioned populations, incubated in S Basal with or
1072 without 2-butanone for 1.5 hours, washed again with S Basal, allowed to
1073 chemotax for two hours on unseeded plates containing two 1 µl spots of 10%
1074 ethanol (blue dots) and 2-butanone diluted in 10% ethanol (orange dots), and
1075 then scored.
1076 (B-E) Chemotaxis indices of (B,D) naïve or (C,E) conditioned wild-type (N2 and
1077 *nIs175*), AIA-ablated (JN580), *nIs175*; *ctbp-1(n4784)*, and *nIs175*; *ctbp-1* mutants
1078 containing a transgene driving expression of wild-type *ctbp-1* under an AIA-
1079 specific promoter (*nIs743[*$P_{gcy\text{-}28.d}$*::ctbp-1(+)]*) at the (B-C) L1 or (D-E) L4 larval
1080 stage. Mean ± SEM. *n* ≥ 6 assays per condition, ≥ 50 worms per assay. ns, not
1081 significant, **p<0.01, ***p<0.001, ****p<0.0001, one-way ANOVA with Tukey's
1082 correction.
1083 (F-G) Chemotaxis indices of (F) naïve or (G) conditioned *nIs175*, *nIs175*; *ctbp-1*,
1084 and *nIs175*; *ctbp-1* mutants carrying the heat-shock-inducible transgene
1085 *nEx2351[*$P_{hsp\text{-}16.2}$*::ctbp-1(+);*$P_{hsp\text{-}16.41}$*::ctbp-1(+)]* with or without heat shock (HS)
1086 at the day 1 adult stage. Mean ± SEM. *n* ≥ 5 assays per condition, ≥ 50 worms
1087 per assay. ns, not significant, **p<0.01, ****p<0.0001, one-way ANOVA with
1088 Tukey's correction.
1089 The *ctbp-1* allele used for all panels of this figure was *n4784*.
1090

Figure 5

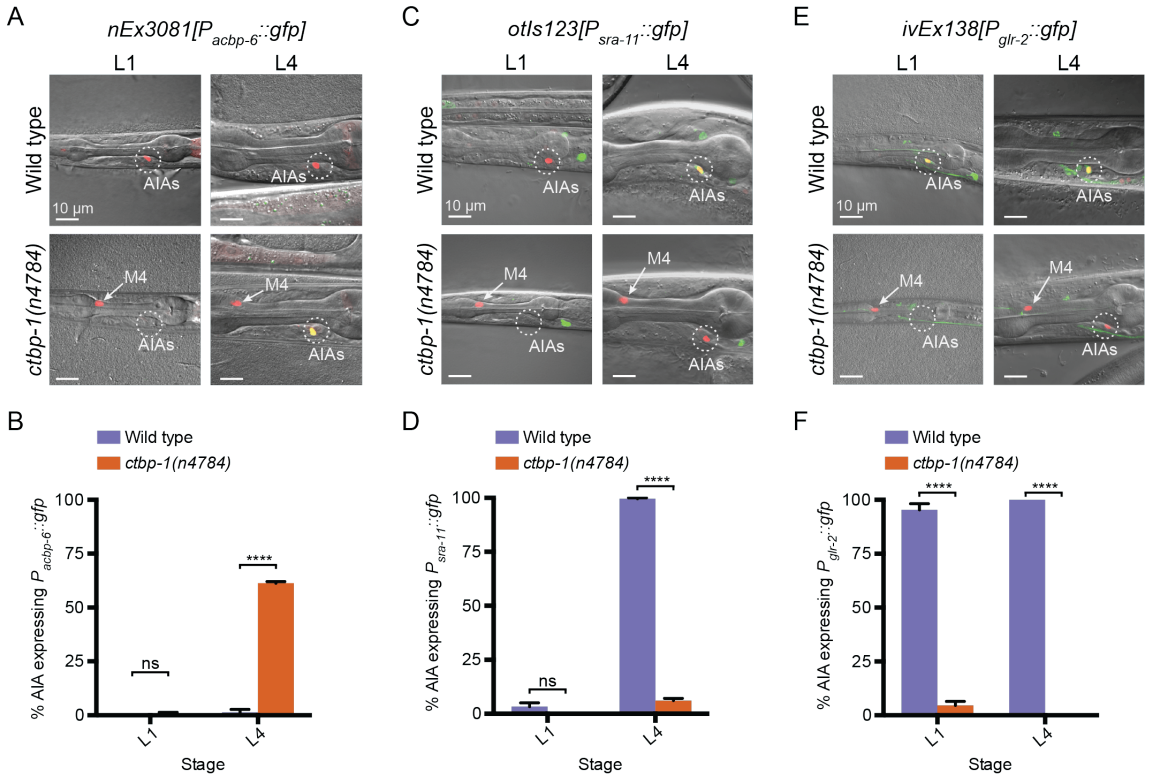

1091

1092 **Figure 5. Loss of *ctbp-1* results in a disruption to normal AIA gene**

1093 **expression**

1094 (A,C,E) (A) *nEx3081[P_{acbp-6}::gfp]*, (C) *otIs123[P_{sra-11}::gfp],* or (E) *ivEx138[P_{glr-}*

1095 *$_{2}$::gfp]* expression in wild-type (top) and *ctbp-1(n4784)* (bottom) worms at the L1

1096 larval stage (left) and L4 larval stage (right). Wild-type strains contain *nIs843[P_{gcy-}*

1097 *$_{28.d}$::mCherry]. ctbp-1* mutant strains contain *nIs348[P_{ceh-28}::mCherry].* Arrow, M4

1098 neuron. Circle, AIAs. Scale bar, 10 µm.

1099 (B,D,F) Percentage of wild-type and *ctbp-1(n4784)* expressing (B) *P_{acbp-6}::gfp*, (D)

1100 *P_{sra-11}::gfp,* or (F) *P_{glr-2}::gfp* in the AIA neurons at L1 and L4 larval stages. Wild-

1101 type strains contain *nIs843[$P_{gcy-28.d}$::mCherry]. ctbp-1* mutant strains contain

1102 *nIs348[P_{ceh-28}::mCherry].* Mean ± SEM. $n \geq 50$ worms per strain per stage, 3

1103 biological replicates. ns, not significant, ****p<0.0001, unpaired t-test.

1104

Figure 6

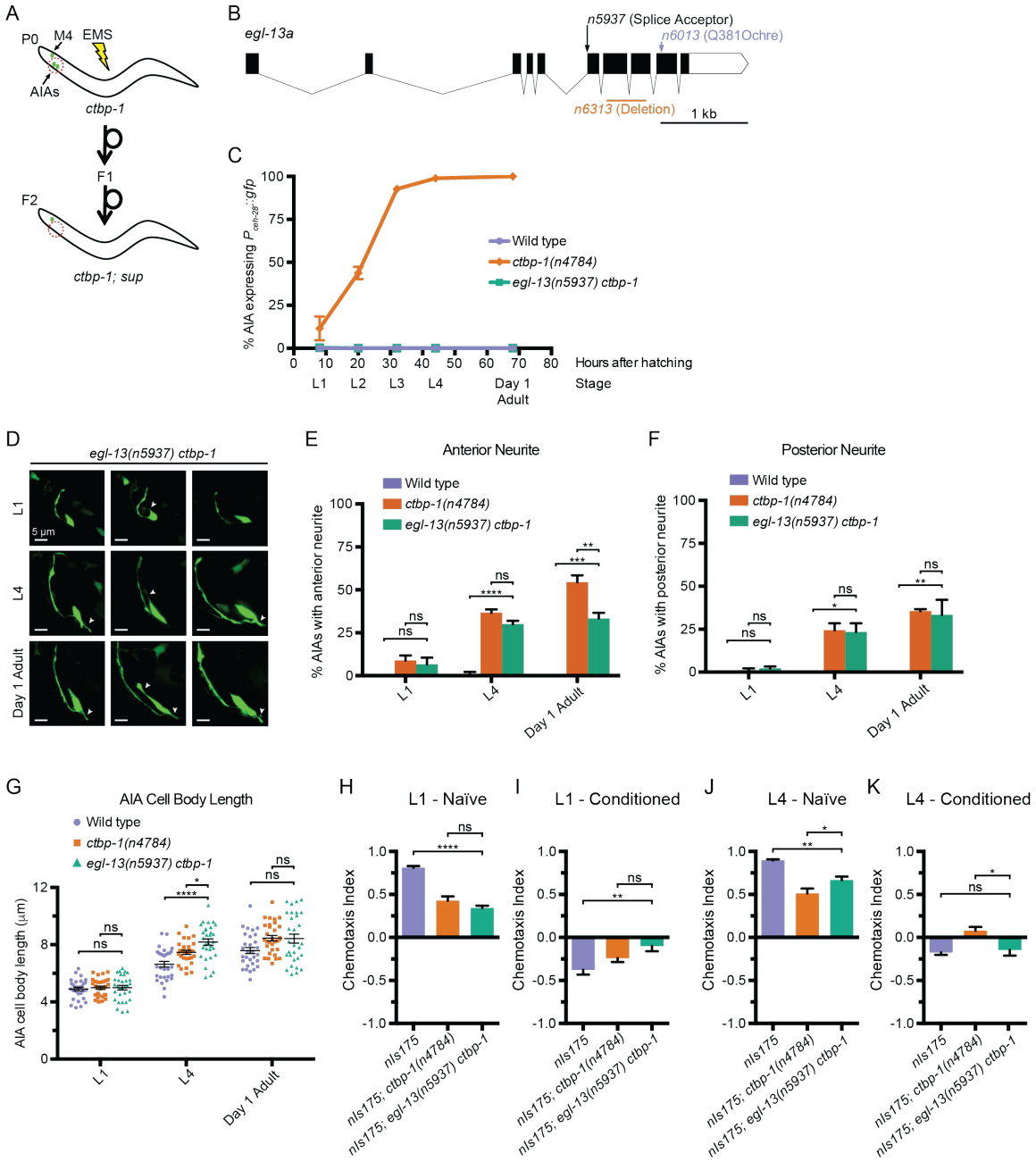

1105

1106 **Figure 6. A suppressor screen reveals *egl-13* as a *ctbp-1* genetic interactor**

1107 (A) Schematic of *ctbp-1* suppressor screen design. *ctbp-1* mutant worms carrying

1108 *nls175[P_{ceh-28}::gfp]* were mutagenized with ethyl methanesulfonate (EMS), and

1109 their F2 progeny were screened for continued *nIs175* expression in M4 and loss
1110 of expression in the AIA neurons (red circle).
1111 (B) Gene diagram of the *egl-13a* isoform. Arrows (above), point mutations. Line
1112 (below), deletion. Scale bar (bottom right), 1 kb.
1113 (C) Percentage of wild-type, *ctbp-1* and *egl-13(n5937)* worms expressing *nIs175*
1114 in the AIA neurons over time. Time points correspond to the L1, L2, L3, L4 larval
1115 stages, and day 1 adult worms (indicated below X axis). All strains contain
1116 *nIs175[*$P_{ceh\text{-}28}$*::gfp].* Mean ± SEM. *n* ≥ 100 worms per strain per stage, 3
1117 biological replicates.
1118 (D) Three representative images of an AIA neuron in *egl-13 ctbp-1* worms at L1
1119 (top), L4 (middle) and day 1 adult (bottom) stages. Arrows, examples of ectopic
1120 neurites protruding from the AIA cell body. Image oriented such that left
1121 corresponds to anterior, top to dorsal. Scale bar, 5 µm.
1122 (E-F) Percentage of AIAs in wild-type, *ctbp-1* and *egl-13 ctbp-1* worms at the L1,
1123 L4 and day 1 adult stages with an ectopic neurite protruding from the (E) anterior
1124 or (F) posterior of the AIA cell body. Mean ± SEM. *n* = 30 AIAs scored per strain
1125 per stage, 3 biological replicates. ns, not significant, *p<0.05, **p<0.01,
1126 ***p<0.001, ****p<0.0001, one-way ANOVA with Tukey's correction.
1127 (G) Quantification of AIA cell body length in wild-type, *ctbp-1* and *egl-13 ctbp-1*
1128 worms at the L1, L4 and day 1 adult stages. Mean ± SEM. *n* ≥ 30 AIAs scored
1129 per strain per stage. ns, not significant, *p<0.05, ****p<0.0001, one-way ANOVA
1130 with Tukey's correction.

1131 (H-K) Chemotaxis indices of (H,J) naïve or (I,K) conditioned wild-type, *ctbp-1* and

1132 *egl-13 ctbp-1* worms at the (H-I) L1 or (J-K) L4 larval stage. Mean ± SEM. $n \geq 5$

1133 assays per condition, ≥ 50 worms per assay. ns, not significant, *p<0.05,

1134 **p<0.01, ****p<0.0001, one-way ANOVA with Tukey's correction.

1135 The *ctbp-1* allele used for all panels of this figure was *n4784*. The *egl-13* allele

1136 used for all panels of this figure was *n5937*.

1137 All strains in (D-G) contain *nIs840[*$P_{gcy\text{-}28.d}$*::gfp]* and all strains in (D-G) other than

1138 "Wild type" contain *nIs348[*$P_{ceh\text{-}28}$*::mCherry]* (not shown in images).

1139 All strains in (C, H-K) contain *nIs175[*$P_{ceh\text{-}28}$*::gfp].*

1140

Figure 7

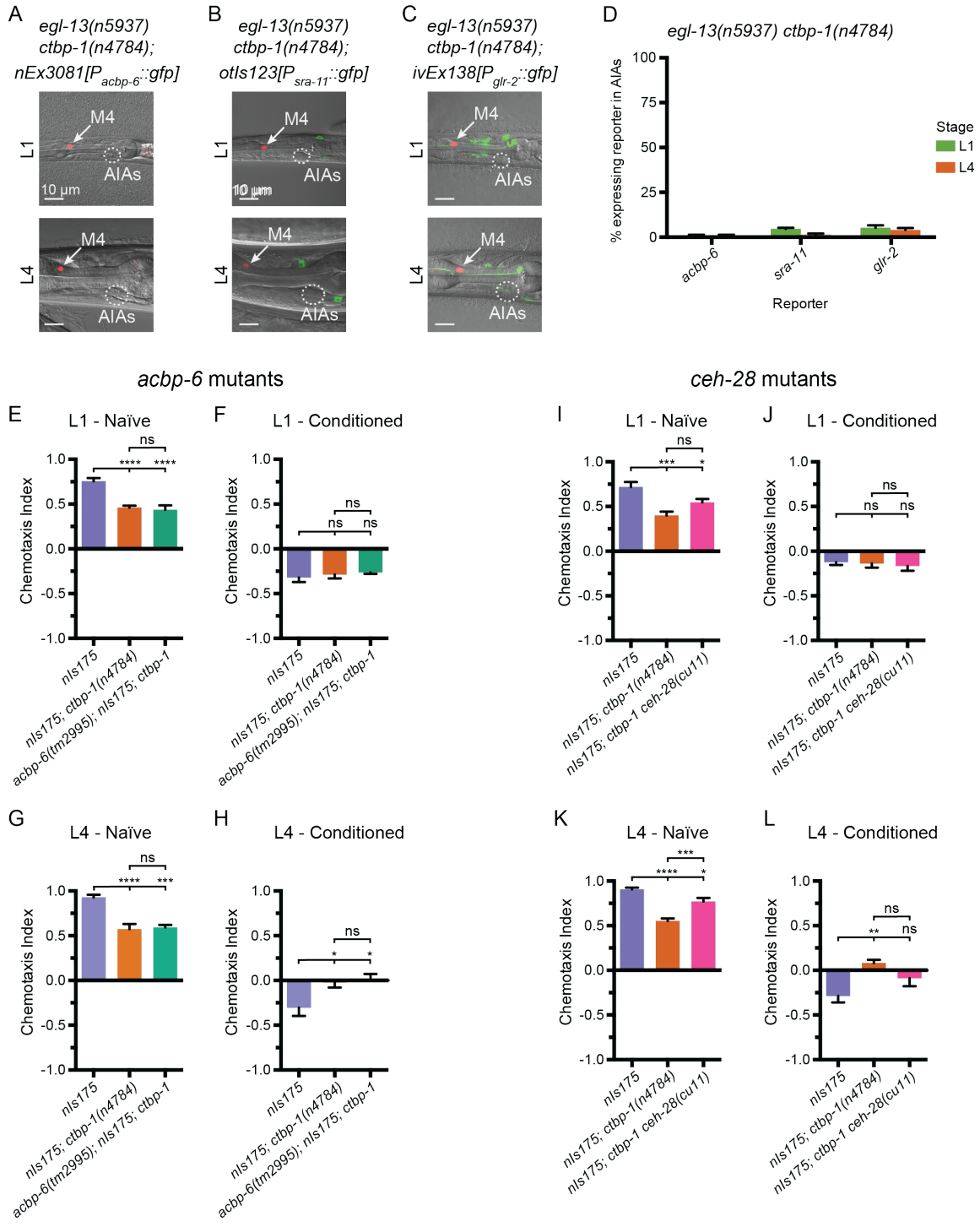

1141

1142 **Figure 7. EGL-13 disrupts AIA function partially through driving**

1143 **misexpression of *ceh-28* in *ctbp-1* mutants**

1144 (A-C) Expression of markers for AIA misexpressed genes (A) *nEx3081[P_{acbp-6}::gfp],* (B) *otIs123[P_{sra-11}::gfp]*, or (C) *ivEx138[P_{glr-2}::gfp]* in *egl-13(n5937) ctbp-*
1145
1146 *1(n4784)* double mutants at the (top) L1 and (bottom) L4 larval stages. Arrow, M4
1147 neuron. Circle, AIAs. Scale bar, 10 µm.
1148 (D) Percentage of *egl-13(n5937) ctbp-1(n4784)* double mutants expressing the
1149 indicated reporter in the AIA neurons at the L1 and L4 larval stages. Mean ±
1150 SEM. *n* ≥ 50 worms scored per strain, 3 biological replicates.
1151 (E-H) Chemotaxis indices of (E,G) naïve or (F,H) conditioned wild-type (*nIs175*),
1152 *nIs175; ctbp-1(n4784)*, and *acbp-6(tm2995)*; *nIs175; ctbp-1* mutants at the (E-F)
1153 L1 or (G-H) L4 larval stage. Mean ± SEM. *n* ≥ 6 assays per condition, ≥ 50
1154 worms per assay. ns, not significant, *p<0.05, ***p<0.001, ****p<0.0001, one-way
1155 ANOVA with Tukey's correction.
1156 (I-L) Chemotaxis indices of (I,K) naïve or (J,L) conditioned wild-type (*nIs175*),
1157 *nIs175; ctbp-1(n4784)*, and *nIs175; ctbp-1 ceh-28(cu11)* mutants at the (I-J) L1
1158 or (K-L) L4 larval stage. Mean ± SEM. *n* ≥ 6 assays per condition, ≥ 50 worms
1159 per assay. ns, not significant, *p<0.05, ***p<0.001, one-way ANOVA with Tukey's
1160 correction.
1161 The *ctbp-1* allele used for all panels of this figure was *n4784.*
1162 All strains in Fig. 7A-D contain *nIs348[P_{ceh-28}::mCherry].*
1163 Images are oriented such that left corresponds to anterior, top to dorsal.
1164

Figure 8

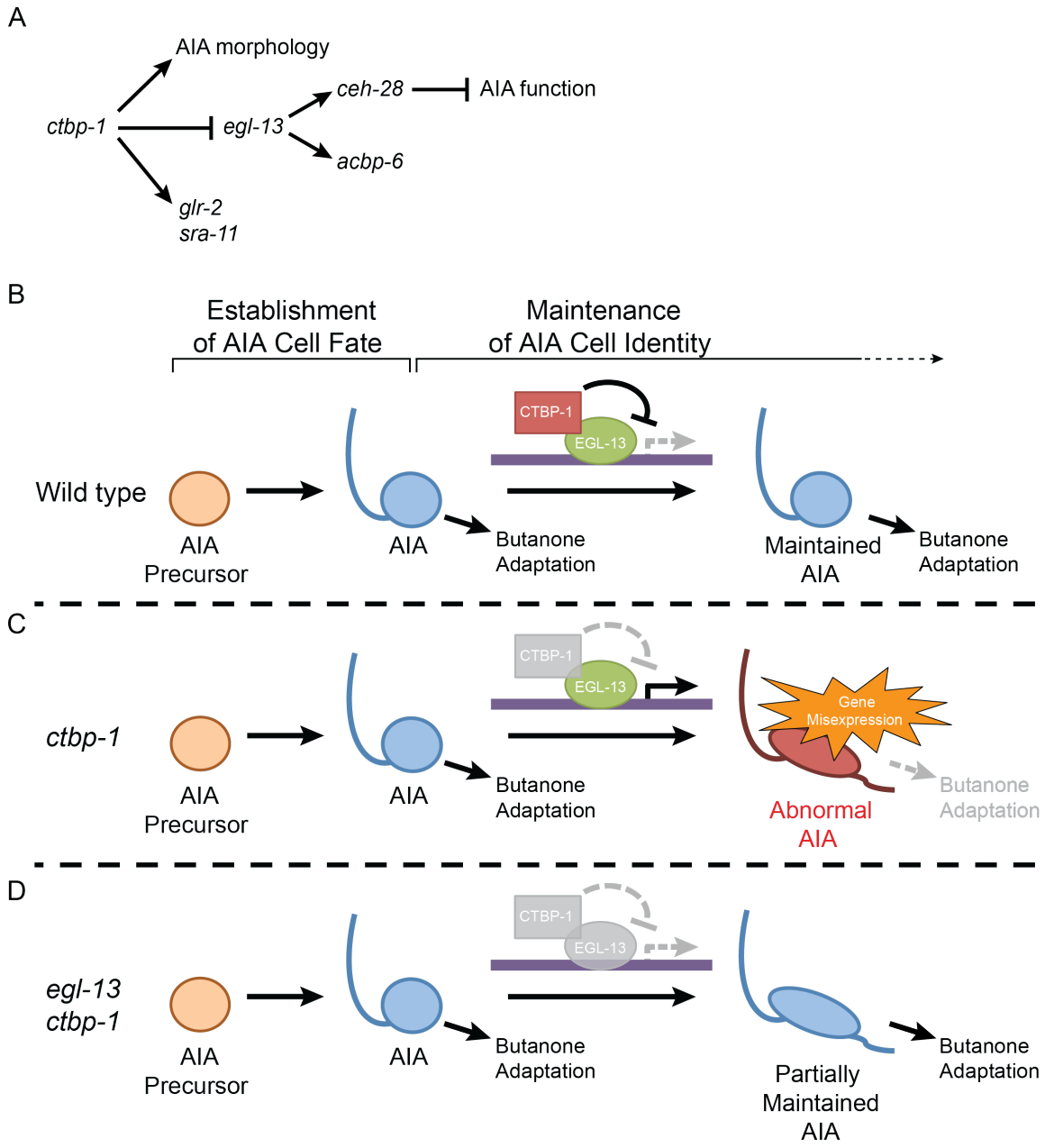

Figure 8. Model for the maintenance of the AIA cell identity by *ctbp-1*

(A) The genetic pathway in which *ctbp-1* promotes AIA morphology and *glr-2* and *sra-11* expression. *ctbp-1* also inhibits *egl-13*, thereby repressing expression of *ceh-28* and *acbp-6* in the AIAs and promoting proper AIA function

(B-D) Model for how CTBP-1 maintains the AIA cell identity.

1171 (B) We propose that CTBP-1 acts in the maintenance but not establishment of
1172 the AIA cell identity, and does so by targeting specific genetic loci for regulation
1173 through physical interaction with transcription factors such as EGL-13.
1174 (C) In the absence of CTBP-1, EGL-13 and other CTBP-1 targets drive
1175 expression at multiple genetic loci, resulting in changes to the gene expression,
1176 morphology and function (as assessed by butanone adaptation) of the AIAs.
1177 (D) When EGL-13 activity is also removed, gene expression and cellular function
1178 are no longer perturbed, while normal morphology is not restored, resulting in a
1179 "Partially Maintained AIA."
1180

Figure S1

A

Allele	Nucleotide Change	Amino Acid Change	Codon Position
n4778	83 bp deletion, frameshift	-	389-417
n4784	CGA to TGA	R → Opal	27
n4789	AGg to AGa	splice site donor	370
n4800	706 bp deletion, frameshift	-	166-216
n4804	GCA to GTA	A → V	261
n4805	CCA to TCA	P → S	29
n4808	CAC to TAC	H → Y	60
n4810	CGA to TGA	R → Opal	55
n4813	TCA to TAA	S → Ochre	113
n4819	CAG to TAG	Q → Amber	208
n4823	AGg to AGa	splice site donor	486
n4824	CAA to TAA	Q → Ochre	100
n4840	TGG to TGA	W → Opal	470
n4849	CGA to TGA	R → Opal	324
n4852	GGg to GGa	splice site donor	265
n4861	GAA to TAA	E → Ochre	220
n4864	CAA to TAA	Q → Ochre	312
n4865	GGA to AGA	G → R	332

B

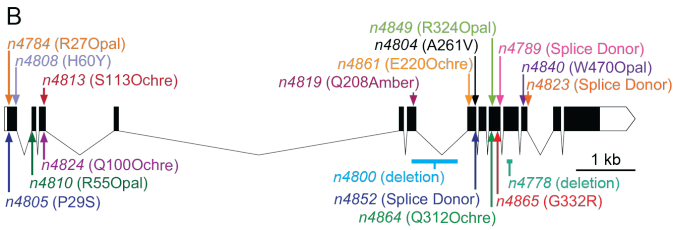

C

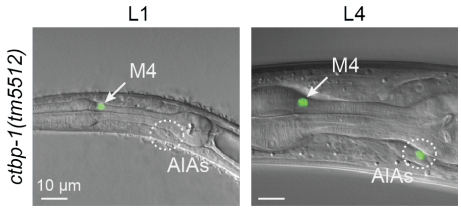

D

nIs175; ctbp-1(tm5512)

Stage	% AIA expressing P_{ceh-28}::*gfp*	*n*
L1	1	100
L4	98	100

E

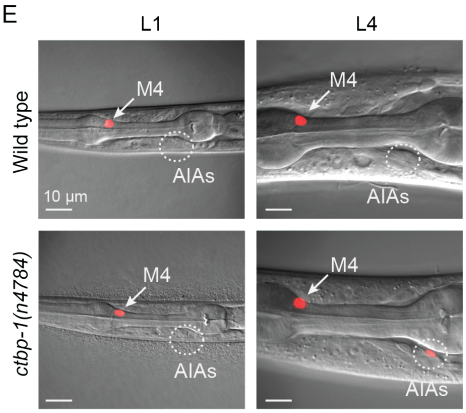

1181

1182 **Figure S1. Additional *ctbp-1* mutant alleles cause misexpression of P_{ceh-28}*::gfp* in the AIA neurons**

1184 (A) Table of *ctbp-1* mutant alleles we showed to result in *nIs175[*P_{ceh-28}*::gfp]* or

1185 *nIs177[*P_{ceh-28}*::gfp]* misexpression in the AIA neurons. Specific nucleotide

1186 changes are denoted in red. Codon positions correspond to the *ctbp-1a* isoform.

1187 (B) Gene diagram of the *ctbp-1a* isoform showing all 18 *ctbp-1* alleles isolated in

1188 this study. Arrows, point mutations. Lines, deletions. Scale bar (bottom right), 1

1189 kb.

1190 (C) Expression of *nIs175* in *ctbp-1(tm5512)* L1 and L4 mutant worms. Arrow, M4

1191 neuron. Circle, AIAs. Scale bar, 10 μm.

1192 (D) Percentage of *ctbp-1(tm5512)* worms expressing *nIs175* in the AIA neurons

1193 at the L1 and L4 larval stages.

1194 (E) *nIs348[*P_{ceh-28}*::mCherry]* expression in wild-type (top) and *ctbp-1(n4784)*

1195 (bottom) worms at the L1 larval stage (left) and L4 larval stage (right). Arrow, M4

1196 neuron. Circle, AIAs. Scale bar, 10 μm.

1197 All strains in Fig. S1A-C contain the either *nIs175[*P_{ceh-28}*::gfp]* or *nIs177[*P_{ceh-28}*::gfp].*

1199 Images are oriented such that left corresponds to anterior, top to dorsal.

1200

Figure S2

A

Genotype	% AIA expressing P_{ceh-28}::*gfp*	*n*
Wild type	0	100
ctbp-1(n4784)	98	100
ctbp-1(n4808)	98	100
ctbp-1(n4784); nEx2346[ctbp-1(+)]	12	100
ctbp-1(n4784); nEx2347[ctbp-1(+)]	4	100
ctbp-1(n4784); nIs743[P_{AIA}::ctbp-1(+)]	0	100

B

ctbp-1(n4784); nEx2351[P_{hsp}::ctbp-1(+)]

Stage	% AIA expressing P_{ceh-28}::*gfp*	*n*
L1	8	100
L4	99	100
Day 1 Adult (- HS)	100	100
Day 1 Adult (+ HS)	8	100

1201

1202 **Figure S2. Quantification of *ctbp-1* strains misexpressing P_{ceh-28}::*gfp***

1203 (A) Percentage of worms of indicated genotypes expressing *nIs175[P_{ceh-28}::gfp]*

1204 in the AIA neurons at the L4 larval stage.

1205 (B) Percentage of *ctbp-1(n4784); nEx2351[$P_{hsp-16.2}$::ctbp-1(+);$P_{hsp-16.41}$::ctbp-1(+)]*

1206 worms expressing *nIs175* at the L1, L4 and day 1 adult stages. Day 1 adults

1207 shown ± heat shock (HS) at the L4 stage.

1208

Figure S3

A

M4 markers

Reporter	Wild type			*ctbp-1(n4784)*		
	% expressing in M4	% expressing in AIAs	*n*	% expressing in M4	% expressing in AIAs	*n*
aylS4	100	0	50	100	0	50
ctlS43	100	0	50	100	0	50
nlS491	100	0	50	100	0	50
ynlS80	100	0	50	100	0	50

B

AIA markers

Reporter	Wild type			*ctbp-1(n4784)*		
	% expressing in M4	% expressing in AIAs	*n*	% expressing in M4	% expressing in AIAs	*n*
nlS843	0	100	50	0	100	50
otlS326	0	100	50	0	100	50
pelS1716	0	100	50	0	100	50
otlS379	0	100	50	0	100	50
otlS317	0	100	50	0	100	50

Figure S3. Quantification of M4 and AIA marker expression

(A-B) Quantification of wild-type and *ctbp-1(n4784)* L4 worms expressing the indicated (A) M4 or (B) AIA markers from Fig. 2A-B in the M4 and AIA neurons.

Figure S4

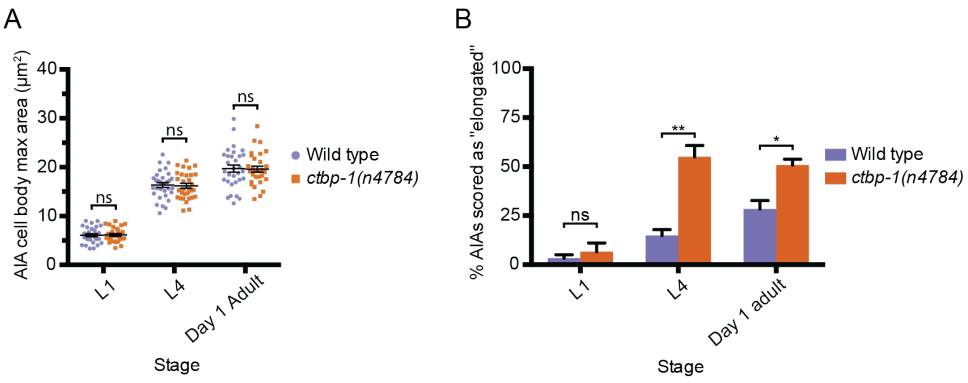

Figure S4. Loss of *ctbp-1* results in a disruption of AIA morphology but not AIA size

1217 (A) Quantification of maximum AIA cell body area in wild-type and *ctbp-1(n4784)*

1218 worms at L1, L4 and day 1 adult stages. Both strains contain *nIs840[*$P_{gcy\text{-}28.d}$*::gfp]*

1219 and the *ctbp-1* strain contains *nIs348[*$P_{ceh\text{-}28}$*::mCherry]*. Mean ± SEM. *n* ≥ 30

1220 AIAs scored per strain per stage. ns, not significant, unpaired t-test.

1221 (B) Scoring of wild-type and *ctbp-1(n4784)* AIA images at the L1, L4 and day 1

1222 adult stages. A random subset of AIA images used for length measurements in

1223 Fig. 3D, 3H and 3L were blinded and scored as having either "Normal" or

1224 "Elongated" AIA cell bodies. *n* ≥ 20 AIAs scored per strain per stage, 3 replicates.

1225 ns, not significant, *p<0.05, **p<0.01, unpaired t-test.

1226

Figure S5

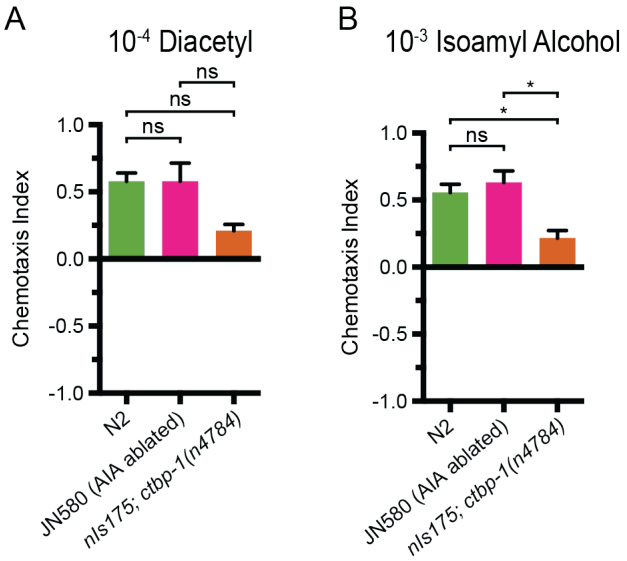

1227

1228 **Figure S5. *ctbp-1* mutants display a non-AIA-dependent chemotaxis defect**

1229 (A-B) Chemotaxis indices of wild-type (N2), AIA-ablated (JN580) and *nIs175*;

1230 *ctbp-1(n4784)* mutants at the L4 larval stage to (A) diacetyl or (B) isoamyl alcohol

1231 diluted in pure ethanol. Mean ± SEM. *n* ≥ 3 assays per condition, ≥ 40 worms per

1232 assay. ns, not significant, *p<0.05, one-way ANOVA with Tukey's correction.

1233

Figure S6

Average Expression (A.U.)		
gene	Wild-type	*ctbp-1*
acbp-6	0.572	13.667
ceh-28	0	4.349
glr-2	0.208	0
sra-11	0.052	0

1234

1235 **Figure S6. Gene expression in wild-type and *ctbp-1* AIAs**

1236 Average expression level of confirmed scRNA-Seq hits in the AIAs of L4 wild-

1237 type and *ctbp-1* mutant animals. A.U., arbitrary expression units.

1238

Figure S7

A

Allele	Nucleotide Change	Amino Acid Change	Codon Position
n5937	gAT to aAT	splice site acceptor	158
n6013	CAA to TAA	Q ➔ Ochre	381
n6313	436 bp deletion	-	205-334

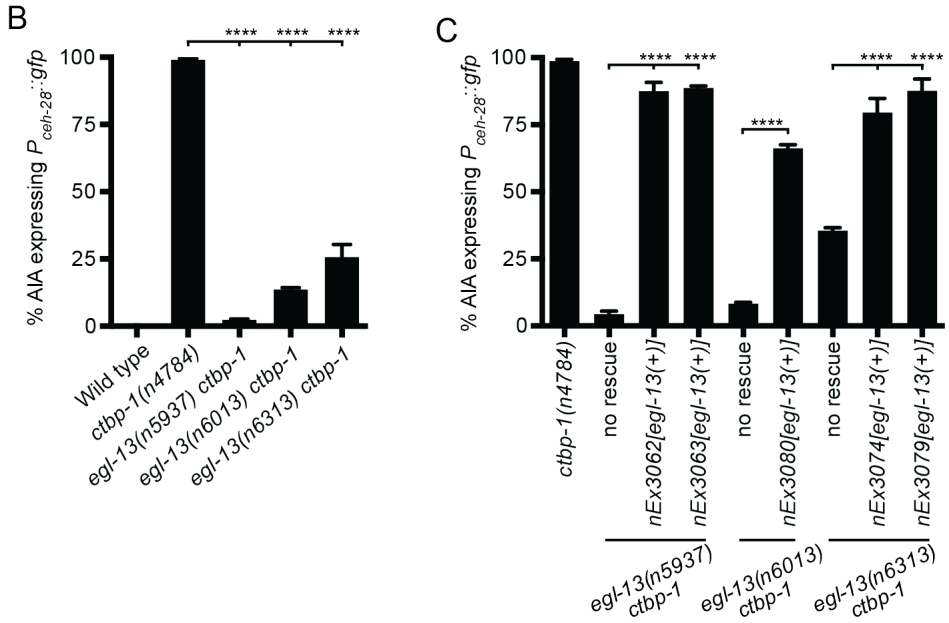

Figure S7. Characterization of *egl-13* alleles isolated as *ctbp-1* suppressors

(A) Table of *egl-13* mutant alleles isolated in this study as suppressors of *ctbp-1*-mediated *nIs175[P_{ceh-28}::gfp]* misexpression in the AIA neurons. Specific nucleotide changes are denoted in red. Codon positions correspond to *egl-13a* isoform.

(B) Percentage of wild-type, *ctbp-1(n4784)* and *egl-13 ctbp-1* worms expressing *nIs175* in the AIA neurons at the L4 larval stage. Mean ± SEM. $n \geq 100$ worms scored per strain, 3 biological replicates. ****$p<0.0001$, one-way ANOVA with Tukey's correction.

1249 (C) Percentage of *ctbp-1(n4784), egl-13 ctbp-1* and *egl-13 ctbp-1* worms carrying

1250 transgenic constructs expressing wild-type *egl-13* under its native promoter

1251 expressing *nIs175* in the AIA neurons at the L4 larval stage. Mean ± SEM. $n \geq 50$

1252 worms scored per strain, 3 biological replicates. ****p<0.0001, one-way ANOVA

1253 with Tukey's correction.

1254 All strains in Fig. S7B-C contain *nIs175[*$P_{ceh\text{-}28}$*::gfp].*

1255

Figure S8

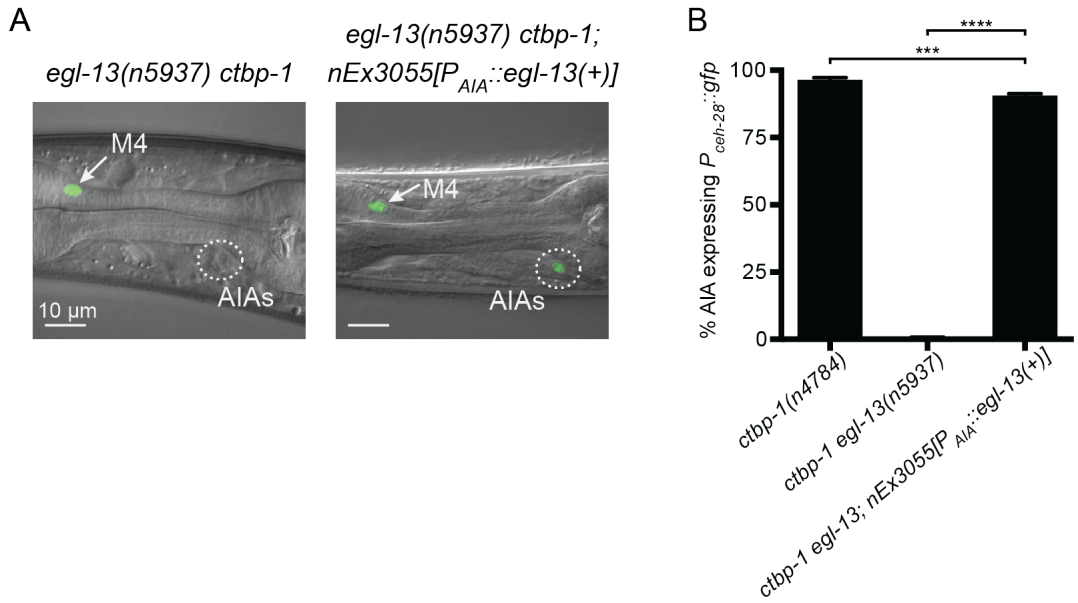

1256

1257 **Figure S8. EGL-13 functions cell-autonomously to regulate AIA gene**

1258 **expression**

1259 (A) Expression of *nIs175[*$P_{ceh\text{-}28}$*::gfp]* in *egl-13(n5937) ctbp-1(n4784)* (left panel),

1260 and *egl-13 ctbp-1* mutants carrying an extrachromosomal array expressing wild-

1261 type *egl-13* under the AIA-specific promoter *gcy-28.d* (*nEx3055*, right panel) in L4

1262 worms. Arrow, M4 neuron. Circle, AIAs. Scale bar, 10 µm.

1263 (B) Percentage of *ctbp-1(n4784)*, *egl-13(n5937) ctbp-1* and *egl-13 ctbp-1;*

1264 *nEx3055* worms expressing *nIs175* in the AIA neurons at the L4 larval stage. All

1265 strains contain *nIs175[*$P_{ceh\text{-}28}$*::gfp].* Mean ± SEM. *n* = 100 worms scored per

1266 strain, 3 biological replicates. ***p<0.001, ****p<0.0001, one-way ANOVA with

1267 Tukey's correction.

1268 The alleles used for all panels of this figure were *ctbp-1(n4784*) and *egl-*

1269 *13(n5937)*.

1270 All strains contain *nIs175[*$P_{ceh\text{-}28}$*::gfp].*

1271 Images are oriented such that left corresponds to anterior, top to dorsal.